



**HAL**  
open science

# Seismoelectric response of heavy oil reservoirs: theory and numerical modelling

A. Revil, Abderrahim Jardani

► **To cite this version:**

A. Revil, Abderrahim Jardani. Seismoelectric response of heavy oil reservoirs: theory and numerical modelling. *Geophysical Journal International*, 2010, 180 (2), pp.781 - 797. 10.1111/j.1365-246X.2009.04439.x . hal-00491086

**HAL Id: hal-00491086**

**<https://hal.science/hal-00491086>**

Submitted on 18 Jun 2021

**HAL** is a multi-disciplinary open access archive for the deposit and dissemination of scientific research documents, whether they are published or not. The documents may come from teaching and research institutions in France or abroad, or from public or private research centers.

L'archive ouverte pluridisciplinaire **HAL**, est destinée au dépôt et à la diffusion de documents scientifiques de niveau recherche, publiés ou non, émanant des établissements d'enseignement et de recherche français ou étrangers, des laboratoires publics ou privés.

# Seismoelectric response of heavy oil reservoirs: theory and numerical modelling

A. Revil<sup>1,2</sup> and A. Jardani<sup>1\*</sup>

<sup>1</sup>Colorado School of Mines, Department of Geophysics, Green Center, 1500 Illinois street, 80401 Golden, CO, USA. E-mail: arevil@mines.edu

<sup>2</sup>LGIT, UMR 5559, CNRS, Equipe Volcan, Université de Savoie, 73376 Le Bourget-du-lac Cedex, France

Accepted 2009 October 29. Received 2009 August 13; in original form 2009 February 1

## SUMMARY

We consider a linear poroelastic material filled with a linear viscoelastic solvent like wet heavy oils (oil as opposed to water or brines is wetting the surfaces of the pores). We extend the electrokinetic theory in the frequency domain accounting for the relaxation effects associated with resonance of the viscoelastic fluid. The fluid is described by a generalized Maxwell rheology with a distribution of relaxation times given by a Cole–Cole distribution. We use the assumption that the charges of the diffuse layer are uniformly distributed in the pore space (Donnan model). The macroscopic constitutive equations of transport for the seepage velocity and the current density have the form of coupled Darcy and Ohm equations with frequency-dependent material properties. These equations are combined with an extended Frenkel–Biot model describing the deformation of the poroelastic material filled with the viscoelastic fluid. In the mechanical constitutive equations, the effective shear modulus is frequency dependent. An amplification of the seismoelectric conversion is expected in the frequency band where resonance of the generalized Maxwell fluid occurs. The seismic and seismoelectric equations are modelled using a finite element code with PML boundary conditions. We found that the DC-value of the streaming potential coupling coefficient is also very high. These results have applications regarding the development of new non-intrusive methods to characterize shallow heavy oil reservoirs in tar sands and DNAPL contaminant plumes in shallow aquifers.

**Key words:** Electrical properties; Electromagnetic theory; Magnetic and electrical properties; Hydrogeophysics.

## 1 INTRODUCTION

In the last 70 yr, a number of laboratory, field, and theoretical investigations have established seismoelectric (seismic-to-electric) and electroseismic (electric-to-seismic) conversions associated with the charged nature of natural and synthetic porous materials filled with a solvent (usually a Newtonian electrolyte). Preliminary investigations have attempted to image the subsurface and to locate potential oil and gas reservoirs and ore bodies using these properties (Martner & Spark 1959; Migunov & Kokorev 1977; Kopic *et al.* 1995; Russell *et al.* 1997). These methods were also used more recently in hydrogeophysics to detect wet ice in glaciers (Kulesa *et al.* 2006), to localize fractures in a fractured aquifer (Fourie 2003), to image interfaces within the vadose zone (Dupuis *et al.* 2007), and to monitor electromagnetic disturbances associated with earthquakes (see Nagao *et al.* 2002; Huang 2002; Huang & Liu 2006). Measurements can be performed not only at the ground surface of the Earth

but also in boreholes (e.g. Butler *et al.* 1996; Mikhailov *et al.* 1997, 2000; Zhu & Toksoz 1998).

Neev & Yeatts (1989) proposed a macroscopic model of the coupling between mechanical waves and electric fields in linear poroelastic materials filled with a Newtonian electrolyte. However, because their work was not based on the full set of Maxwell equations, they were not able to compute correctly electromagnetic disturbances associated with shear waves. Pride (1994) completed the theory for a charged porous material filled with water by upscaling the local Navier–Stokes and Nernst–Planck equations using a volume-averaging method to obtain the macroscopic equations. His theory connects the Frenkel–Biot poroelastic equations (Frenkel 1944; Biot 1962a,b) and the Maxwell–Lorentz equations (Maxwell 1885; Lorentz 1904) through the electrokinetic coupling occurring in the constitutive equations for the fluxes of water and current density (see Garambois & Dietrich 2001, 2002). In doing so, he also accounted for frequency dependence of the material properties entering the coupled transport constitutive equations.

This paper is an attempt to provide a constitutive model of the seismoelectric response of a charged porous medium filled with a (Maxwell) viscoelastic solvent like a heavy wet-oil. They are

\*Now at: M2C, UMR 6143, CNRS, Morphodynamique Continentale et Côtière, Université de Rouen, 76821 Mont Saint Aignan, France.

numerous examples in the literature where oil is the wetting phase for the solid grains (see Anderson 1986; Buckley & Liu 1998, for some field examples). We are not aware of any work in this direction so far. At low frequencies, it has been observed that electrokinetic phenomena in oil-wet porous media are similar to those existing in water-saturated porous materials (Yasufuku *et al.* 1977; Alkafef *et al.* 2001; Alkafef & Smith 2005). Various authors have shown that the components of oil that are responsible for wettability are also polar components (Buckley & Liu 1998; Alkafef *et al.* 2006). An oil with such polar molecules is also a good solvent (Delgado *et al.* 2007). We will show that the theory developed in this paper is also consistent with recent developments in the theory of streaming current/streaming potential associated with the flow of the pore water in a deformable porous material (see Revil & Linde 2006; Crespy *et al.* 2008).

## 2 PROPERTIES OF THE TWO PHASES

### 2.1 Properties of the fluid phase

We start this section by a description of the constitutive model of the stress–strain relationships for a viscoelastic fluid such as a wet-oil. A linear Maxwell fluid model consists of a linear dashpot in series with a linear spring. In this situation, the fluid behaves like a Newtonian viscous fluid at low frequency (or for long timescales) and like a solid at high frequencies (or short timescales) (Behura *et al.* 2007). The transition frequency is discussed below. We note  $T_{ij}$  and  $e_{ij}$  the components of the stress and deformation tensors  $\mathbf{T}_f$  and  $\mathbf{e}_f$  of this fluid (subscript  $f$ ), respectively. Both  $\mathbf{T}_f$  and  $\mathbf{e}_f$  are symmetric second-order tensors. The stress components of the elastic and viscous contributions of the Maxwell fluid are given by

$$(T_{ij})^e = \lambda_f (e_{kk})^e \delta_{ij} + 2G_f (e_{ij})^e, \quad (1)$$

$$(T_{ij})^v = 2\eta_f (\dot{e}_{ij})^v - p_f \delta_{ij}, \quad (2)$$

where the superscripts ‘ $e$ ’ and ‘ $v$ ’ stands for ‘elastic’ and ‘viscous’ contributions to the stress tensor and to the deformation tensor, the dot above the symbol denotes the first time derivative of the property,  $\lambda_f$  and  $G_f$  are the Lamé and shear moduli of the fluid,  $\eta_f$  is the dynamic (shear) viscosity and  $p_f$  is the local fluid pressure.

The bulk modulus of the fluid is defined by the relationship  $-p_f \mathbf{I} = K_f (\nabla \cdot \mathbf{u}_f) \mathbf{I}$  where  $\mathbf{I}$  is the identity tensor and  $\mathbf{u}_f$  is the displacement of the fluid phase. It is related to the Lamé constants by  $K_f = \lambda_f + (2/3)G_f$ . For a Maxwell body, the components of the stress tensor of the fluid,  $\mathbf{T}_f$ , are given by  $T_{ij} = (T_{ij})^e = (T_{ij})^v$  and  $\dot{e}_{ij} = (\dot{e}_{ij})^e + (\dot{e}_{ij})^v$ . Using eqs (1) and (2) into  $\dot{e}_{ij} = (\dot{e}_{ij})^e + (\dot{e}_{ij})^v$  yields

$$\dot{T}_{ij} + \frac{G_f}{\eta_f} (T_{ij} + p_f \delta_{ij}) = 2G_f \dot{e}_{ij} + \lambda_f (\dot{e}_{kk})^e \delta_{ij}. \quad (3)$$

Using harmonic variations of the stress (the stress oscillates in time as  $e^{-i\omega t}$ ), we can take the previous equation in the frequency domain using a Fourier transform (we keep however the same notations). The characteristic frequency is defined as  $\omega_m = G_f/\eta_f$  and the associated relaxation time is  $\tau_m = \eta_f/G_f$ . Typically, for the Mexican crude oil investigated by Dante *et al.* (2007), the critical frequency depends on the temperature and is in the range 10–100 Hz in the temperature range 20–40 °C. For heavy oils in tar sands for example, the critical frequency of resonance can occur at much lower frequencies. Usually, heavy oils are heated to decrease their dynamic viscosity and the resonance frequency can occur in the seismic frequency band (see Behura *et al.* 2007).

In the frequency domain, eq. (3) is written as,

$$T_{ij} = -p_f^* \delta_{ij} + 2\eta_f^* (-i\omega e_{ij})^v - \frac{i\omega\tau_m}{1 - i\omega\tau_m} [\lambda_f (e_{kk})^e \delta_{ij} + 2G_f (e_{ij})^e], \quad (4)$$

$$p_f^* = \frac{p_f}{1 - i\omega\tau_m}, \quad (5)$$

$$\eta_f^* = \frac{\eta_f}{1 - i\omega\tau_m}. \quad (6)$$

At low frequencies  $\omega \ll \omega_m$  so that  $p_f^* = p_f$ ,  $\eta_f^* = \eta_f$ , the third term on the right-hand side of eq. (4) is negligible and the stress tensor is given by (e.g. De Groot & Mazur 1984)

$$\mathbf{T}_f = K_f (\nabla \cdot \mathbf{u}_f) \mathbf{I} + 2\eta_f (\dot{\mathbf{d}}_f)^v, \quad (7)$$

where the  $(\dot{\mathbf{d}}_f)^v$  is the viscous contribution to the fluid strain deviator (e.g. De Groot & Mazur 1984),

$$(\dot{\mathbf{d}}_f)^v = \frac{1}{2} [\nabla \mathbf{v}_f + (\nabla \mathbf{v}_f)^T] - \frac{1}{3} (\nabla \cdot \mathbf{v}_f) \mathbf{I}, \quad (8)$$

where  $\mathbf{d}_f$  is the fluid strain deviator,  $\mathbf{v}_f$  denotes the velocity of the fluid and where the superscript  $T$  means transpose. The deformation tensor is related to the deviator by (e.g. De Groot & Mazur 1984),

$$\mathbf{e}_f = (1/3) (\nabla \cdot \mathbf{u}_f) \mathbf{I} + \mathbf{d}_f. \quad (9)$$

At low frequencies the fluid behaves like a Newtonian fluid.

At high frequencies  $\omega \gg \omega_m$ , the stress tensor is given by

$$\mathbf{T}_f = K_f (\nabla \cdot \mathbf{u}_f) \mathbf{I} + 2G_f \mathbf{d}_f, \quad (10)$$

and therefore at high frequencies the pore fluid behaves as a solid.

A perfect Maxwell fluid has a relaxation time distribution described by a delta function. Such a model can be generalized using a distribution of relaxation times, for example a Cole–Cole distribution [see for example, Revil *et al.* (2006) for deformation of rocks by pressure solution, Cosenza *et al.* (2007) for spectral induced polarization]. Behura *et al.* (2007) used a Cole–Cole model to fit the hydromechanical behaviour of the Uvalde heavy-oil. A comparison between the Maxwell and Cole–Cole behaviour of the resonances of a generalized Maxwell fluid is shown in Fig. 1 where we compare experimental data from Castrejon-Pita *et al.* (2003) for a Maxwell fluid (a mixture of cetylpyridinium chloride and sodium salicylate) with a model in which the Cole–Cole distribution of relaxation times is used. From this figure, it can be concluded that the Cole–Cole model is able to represent the hydrodynamic behaviour of the fluid quite well. The probability distribution (normalized) of the relaxation time for a Cole–Cole distribution is given by (Cole & Cole 1941)

$$f(\tau) = \frac{1}{2\pi} \frac{\sin[\pi(c-1)]}{\cosh[c \ln(\tau/\tau_m)] - \cos[\pi(c-1)]}. \quad (11)$$

In a semi-log plot, this distribution is symmetric with respect to  $\tau = \tau_m$ , which corresponds to the peak of the distribution. For  $0.5 \leq c \leq 1$ , the Cole–Cole distribution of relaxation times looks like a log normal distribution. The tail of the Cole–Cole distribution is however increasingly broad as  $c$  decreases. This type of distribution has been used recently by Leroy *et al.* (2008) and Leroy & Revil (2009) to model the grain size distribution of packs of glass beads and sedimentary rocks to compute their complex resistivity.

The behaviour of the Maxwell fluid can be considered from the standpoint of the behaviour of an equivalent Newtonian viscous

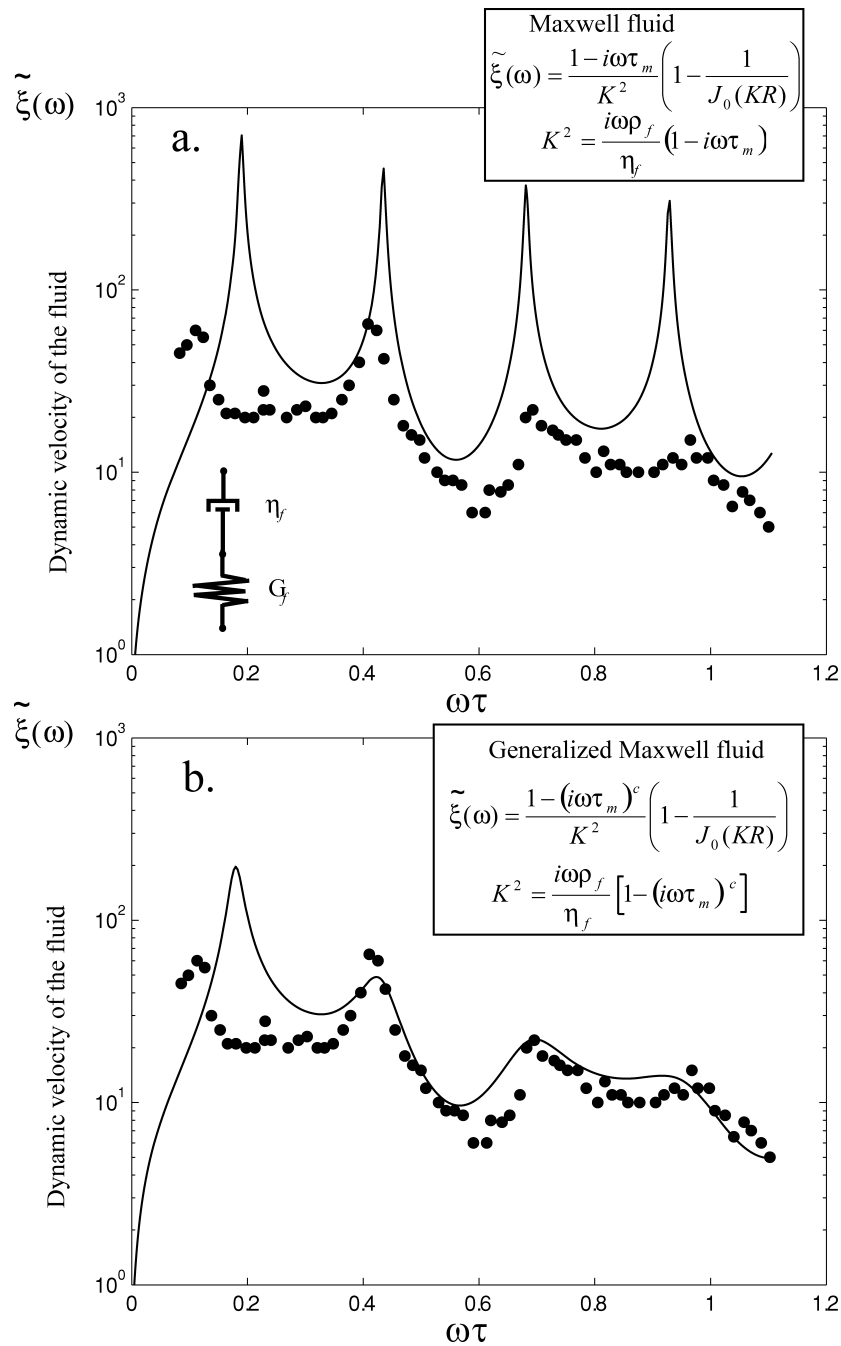


**Figure 1.** Hydrodynamic response of a viscoelastic fluid in a linear tube of radius  $R = 2.5$  cm submitted to harmonic fluid pressure variations. The fluid is a mixture of cetylpyridinium chloride and sodium salicylate (CPyCl/NaSal 60:100) (data from Castrejon-Pita *et al.* 2003). The experimental data are scaled with respect to the viscous relaxation time  $\tau = R^2\rho_f/\eta_f$  ( $\eta_f = 60$  Pa s,  $\rho_f = 1050$  kg m $^{-3}$ ).  $\tilde{\xi}$  denotes the normalized conductance (relative to the DC-value) and  $J_0$  is the Bessel function. (a) Comparison between the experimental data and the response predicted by a linear Maxwell fluid ( $\tau_m = 1.9$  s). (b) Comparison between the experimental data and the response predicted by a generalized Maxwell fluid using a Cole–Cole distribution of relaxation times ( $\tau_m = 2.9$  s, Cole–Cole exponent  $c = 0.9$ , parameters optimized with a Newton–Raphson minimization method using the  $L_2$ -norm).

fluid with frequency dependent bulk modulus and dynamic shear viscosity (Behura *et al.* 2007)

$$\mathbf{T}_f = K_f^*(\omega)(\nabla \cdot \mathbf{u}_f)\mathbf{I} + 2\eta_f^*(\omega)(\dot{\mathbf{d}}_f)^v - \frac{(i\omega\tau_m)^c}{1 - (i\omega\tau_m)^c} [K_f(\nabla \cdot \mathbf{u}_f)\mathbf{I} + 2G_f(\dot{\mathbf{d}}_f)^c], \quad (12)$$

$$K_f^*(\omega) = \frac{K_f}{1 - (i\omega/\omega_m)^c}, \quad (13)$$

$$K_f^*(\omega)(\nabla \cdot \mathbf{u}_f) = -p_f^*, \quad (14)$$

$$p_f^*(\omega) = \frac{P_f}{1 - (i\omega/\omega_m)^c}, \quad (15)$$

$$\eta_f^*(\omega) = \frac{\eta_f}{1 - (i\omega/\omega_m)^c}. \quad (16)$$

Using Boussinesq approximation, the flow of a fluid inside a deformable porous material is governed locally by the Navier–Stokes

equation,

$$\rho_f \frac{\partial \mathbf{v}_f}{\partial t} = -\nabla p_f + \nabla \cdot \boldsymbol{\pi} + \mathbf{F}_f, \quad (17)$$

$$\nabla \cdot \mathbf{v}_f = 0, \quad (18)$$

respectively, where  $\rho_f$  denote the local mass density of the fluid,  $\mathbf{F}_f$  is the body force, and

$$\boldsymbol{\pi} = \mathbf{T}_f + p_f^* \mathbf{I} + \frac{i\omega\tau_m}{1 - i\omega\tau_m} [K_f(\nabla \cdot \mathbf{u}_f)\mathbf{I} + 2G_f(\mathbf{d}_f)^e], \quad (19)$$

represents the viscous (deviatoric) stress tensor of the fluid. For a purely viscous Newtonian fluid, we have  $\nabla \cdot \boldsymbol{\pi} = \eta_f \nabla^2 \mathbf{v}_f$ . Assuming a linearized Maxwell model and using eq. (4), the viscous stress tensor  $\boldsymbol{\pi}$  is given by

$$\dot{\boldsymbol{\pi}} + \left(\frac{G_f}{\eta_f}\right) \boldsymbol{\pi} = 2G_f \dot{\mathbf{d}}_f, \quad (20)$$

$$\tau_m \dot{\boldsymbol{\pi}} + \boldsymbol{\pi} = \eta_f \nabla \mathbf{v}_f. \quad (21)$$

In the frequency domain, eq. (21) yields

$$(1 - i\omega\tau_m)\boldsymbol{\pi} = \eta_f \nabla \mathbf{v}_f, \quad (22)$$

$$\nabla \cdot \boldsymbol{\pi} = \frac{\eta_f}{1 - i\omega\tau_m} \nabla^2 \mathbf{v}_f. \quad (23)$$

Inserting eq. (23) inside the Navier–Stokes equation, eq. (17), yields

$$-i\omega\rho_f \mathbf{v}_f = -\nabla p_f + \eta_f^* \nabla^2 \mathbf{v}_f + \mathbf{F}_f. \quad (24)$$

Consequently, we come to the important conclusion that the Navier–Stokes equation of a viscous Newtonian fluid can be used by replacing the classical viscosity  $\eta_f$  by an effective (time or frequency dependent) viscosity  $\eta_f^*$ . This is the main result of this section with the new result of using a Cole–Cole distribution of relaxation times to describe a generalized Maxwell fluid (see Fig. 1b).

## 2.2 Properties of the solid phase

We consider that the solid phase is formed by a monomineralic isotropic solid material assumed to be perfectly elastic. The local elastic equation of motion for the solid phase is

$$\nabla \cdot \mathbf{T}_s + \mathbf{F}_s = \rho_s \frac{\partial^2 \mathbf{u}_s}{\partial t^2}. \quad (25)$$

where  $\mathbf{u}_s$  is the displacement of the solid phase,  $\rho_s$  is the bulk density of the solid phase and  $\mathbf{F}_s$  is the body force applied to the grains. The microscopic solid stress tensor is given by

$$\mathbf{T}_s = K_s (\nabla \cdot \mathbf{u}_s) \mathbf{I} + 2G_s \mathbf{d}_s, \quad (26)$$

$$\mathbf{d}_s = \frac{1}{2} [\nabla \mathbf{u}_s + \nabla \mathbf{u}_s^T] - \frac{1}{3} (\nabla \cdot \mathbf{u}_s) \mathbf{I}, \quad (27)$$

where  $\mathbf{d}_s$  is the solid strain deviator,  $K_s$  is the bulk modulus of the solid phase assumed to be isotropic and  $G_s$  is the shear modulus.

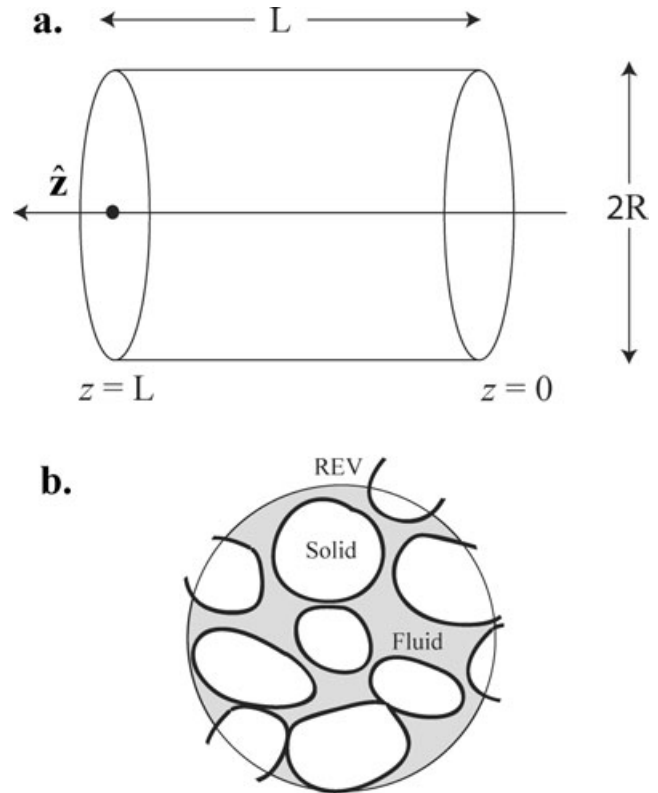


**Figure 2.** Sketch of the porous material. (a) The representative elementary volume is an averaging disc of radius  $R$  and length  $L$ . (b) The representative elementary volume (REV) corresponds to a porous body filled with a viscoelastic fluid.

## 3 PROPERTIES OF THE POROUS MATERIAL

We derived below the coupled constitutive equations between the Darcy velocity (Section 3.1) and the total current density (Section 3.2) for a linear poroelastic material saturated by a polar (wet) oil (Fig. 2).

We look for an average force balance equation on the fluid in relative motion with respect to the solid phase. We introduce the relative flow velocity  $\mathbf{v} = \mathbf{v}_f - \bar{\mathbf{v}}_s$  where  $\bar{\mathbf{v}}_s = \dot{\mathbf{u}}_s$  is the phase averaged velocity of the solid phase. In the frequency domain, using eq. (24) yields

$$-i\omega\rho_f \mathbf{v} = -\nabla p_f + i\omega\rho_f \bar{\mathbf{v}}_s + \eta_f^* \nabla^2 \mathbf{v} + \mathbf{F}_f, \quad (28)$$

$$\eta_f^*(\omega) = \frac{\eta_f}{1 - (i\omega\tau_m)^c}, \quad (29)$$

where  $c$  is the Cole–Cole distribution corresponding to the distribution of the relaxation times for the generalized Maxwell fluid. The body force applied to the pore fluid corresponds to the electrostatic force associated with the existence of the local net charge density  $Q$  (expressed in  $\text{C m}^{-3}$ ) plus the body force due to the gravity field

$$\mathbf{F}_f = \rho_f \mathbf{g} + Q\mathbf{E}e^{-i\omega t}, \quad (30)$$

where  $\rho_f$  is the mass density of the pore water,  $\mathbf{g}$  the acceleration of the gravity and  $\mathbf{E}$  is the electric field. The average force  $\bar{\mathbf{F}}_f$  can be also associated with a source mechanism (see below Section 6.4 and using the decomposition provided by eq. 56). We average now eq. (28) over the fluid phase. This yields

$$-i\omega\rho_f \bar{\mathbf{v}} = -\nabla \bar{p}_f + i\omega\rho_f \bar{\mathbf{v}}_s + \eta_f^* \nabla^2 \bar{\mathbf{v}} + \bar{\mathbf{F}}_f, \quad (31)$$

The flow is also subjected to the no-slip boundary condition  $\bar{\mathbf{v}} = 0$  at the surface of the pores.

The local charge density  $Q$  depends on the position inside the pore space. This local charge density is related to the concentrations of the ionic species that are affected by the Coulombic field created by the effective surface charge density of the mineral surface. These surface concentrations are described by Boltzmann distributions. The electrical double layer is always thin with respect to the size of the pores and the size of the grains. In this paper, we use the approximation developed by Revil & Linde (2006) that  $Q$  can be replaced by its phase average over the fluid phase

$$\bar{Q}_V = \sum_{i=1}^N q_i \bar{C}_i, \quad (32)$$

where  $\bar{C}_i$  is the phase average of the concentration of species  $i$  in the pore space and  $q_i$  the charge (in C) of the ionic species  $i$  ( $q_i = 0$  for neutral species) (see Pride 1994 for the definition of the phase average). This approximation does not mean that we consider that the double layer is thick, but only that the charge distribution is averaged over the pore space. Using this approximation, Revil & Linde (2006) and Revil (2007) have presented recently a model to study electrokinetic properties of deformable porous materials saturated by a viscous (Newtonian) solvent like an aqueous electrolyte. This model was validated through experiments at different scales (Revil *et al.* 2003; Bolève *et al.* 2007; Crespy *et al.* 2008) and generalized to unsaturated conditions by Linde *et al.* (2007) and Revil *et al.* (2007). It has been successfully used recently inside a stochastic framework to determine the flow pattern in geothermal fields (Jardani & Revil 2009).

The charge density  $\bar{Q}_V$  corresponds to the effective charge density of the diffuse layer per unit pore volume that can be carried by the flow of the pore water relative to the mineral framework. The surface charge density  $\bar{Q}_V V_p / S$  ( $V_p$  is a pore volume and  $S$  a surface area of the solid–fluid interface) counterbalances the surface charge density of the mineral surface plus the surface charge density of the Stern layer of sorbed counterions (Leroy *et al.* 2007). The mean charge density of the diffuse layer  $\bar{Q}_V$  can also be related to the total volumetric charge density  $Q_V$  (traditionally determined by cation exchange capacity measurements in water saturated rocks, see Revil *et al.* 1998) by

$$\bar{Q}_V = (1 - f_Q) Q_V, \quad (33)$$

where  $f_Q$  is the fraction of charges located in the Stern layer. The Stern layer is a layer of sorbed counterions on the mineral surface. The surface charge density of the mineral surface is counterbalanced by the surface charge density of the stern plus diffuse layers. The counterions are charges of opposite site to the charge of the mineral surface while the coions have charge of the same charge than the mineral surface. According to the electrochemical models developed by Leroy & Revil (2004) and Leroy *et al.* (2007) for clay minerals, approximately 90 per cent of the counterions are usually located in the Stern layer in the case of Illite and smectite and over 98 per cent in the case of kaolinite. For silica, an electrochemical model has been discussed recently by Leroy *et al.* (2008). This model shows that the fraction  $f_Q$  of counterions located in the Stern layer at the surface of silica grains depends strongly on the salinity (and pH) of the solution. At low salinities ( $\leq 10^{-3}$  mol L<sup>-1</sup>), most of the counterions are located in the diffuse layer while at high salinity ( $> 10^{-3}$  mol L<sup>-1</sup>) the counterions are mainly located in the Stern layer. The situation is different for clays for which  $f_Q$  is much less sensitive to the salinity of the free pore water.

Fig. 3 shows that for a wide range of porous media and for electrolytes of different ionic strengths, the excess of charge per unit pore volume  $\bar{Q}_V$  can be related to the DC-permeability  $k_0$ . While most of the data reported in Fig. 3 concern aqueous electrolytes, a similar trend is expected for wet oils as discussed further at the end of this section.

The boundary value problem for the fluid flow is expressed on an averaging disc (see Pride 1994) by

$$\eta_f^* \nabla^2 \mathbf{v} + i\omega \rho_f \mathbf{v} = \nabla p_f - \mathbf{F}_f, \quad (34)$$

$$\nabla \cdot \mathbf{v} = 0, \quad (35)$$

$$\mathbf{v} = 0 \text{ on } S, \quad (36)$$

$$p_f = \begin{cases} \hat{\mathbf{z}} \cdot (\nabla \bar{p}_f - i\omega \rho_f \hat{\mathbf{u}}_s), & z = L \\ 0, & z = 0 \end{cases}, \quad (37)$$

where  $S$  represents the solid–pore fluid interface and  $\hat{\mathbf{z}}$  is the unit vector normal to the disc face of the representative elementary volume. This boundary-value problem is exactly the same as the boundary-value problem studied by Pride (1994) for a poroelastic porous body saturated by a Newtonian fluid except that  $\eta_f$  should be replaced by  $\eta_f^*$ . We can therefore easily generalize the results obtained by Pride (1994) to a poroelastic material saturated by a viscoelastic solvent. This yields the following modified Darcy equation

$$-i\omega \bar{\mathbf{w}} = \frac{k(\omega)}{\eta_f} [-\nabla \bar{p}_f + \rho_f \omega^2 \bar{\mathbf{u}}_s + \bar{\mathbf{F}}_f] - c(\omega) \sigma \mathbf{E}, \quad (38)$$

where  $\bar{\mathbf{w}} = \phi(\bar{\mathbf{u}}_f - \bar{\mathbf{u}}_s)$  is the filtration displacement of the fluid phase relative to the mineral framework (Darcy velocity),  $\phi$  is the interconnected porosity,  $\bar{\mathbf{w}}(\omega) = \phi \bar{\mathbf{v}}(\omega)$  is the Darcy velocity,  $k(\omega)$  is the dynamic permeability,  $c(\omega)$  is the dynamic coupling coefficient described below and  $\sigma$  is the electrical conductivity of the porous material. The electrical conductivity is given by upscaling the local Nernst–Planck equation. We assume that the wet oil carries a net charge per unit volume to compensate the fixed charge density at the surface of the minerals. In this case, using the Donnan model described by Revil & Linde (2006), the total current density  $\mathbf{j}$  (in A m<sup>-2</sup>) of the porous material is given by  $\mathbf{j} = \sigma \mathbf{E} + \bar{Q}_V \bar{\mathbf{w}}$ . In this equation, the last term corresponds to the source current density given by the product between an effective charge density and the Darcy-velocity. This equation differs from the more conventional form, which employs the product of a cross-coupling coefficient with the gradient of fluid pressure and an inertial coupling term. This approach has much less parameters than the classical approach because the charge density  $\bar{Q}_V$  can be determined from the DC-permeability alone.

At low frequency, the electrical field  $\mathbf{E}$  is related to the electrical potential  $\psi$  by  $\mathbf{E} = -\nabla \psi$  to satisfy  $\nabla \times \mathbf{E} = 0$ . The low-frequency coupling coefficient is given by

$$c_0 = \left( \frac{\partial \psi}{\partial p_f^0} \right)_{j=0} = -\frac{\bar{Q}_V k_0}{\eta_f \sigma}. \quad (39)$$

This equation has been validated on core samples saturated by electrolytic solvents (Revil *et al.* 2005). The electrical conductivity of the porous material is given by (Johnson 1986)

$$\sigma = \frac{1}{F} \left( \bar{\sigma}_f + \frac{2}{\Lambda} \Sigma_s \right), \quad (40)$$

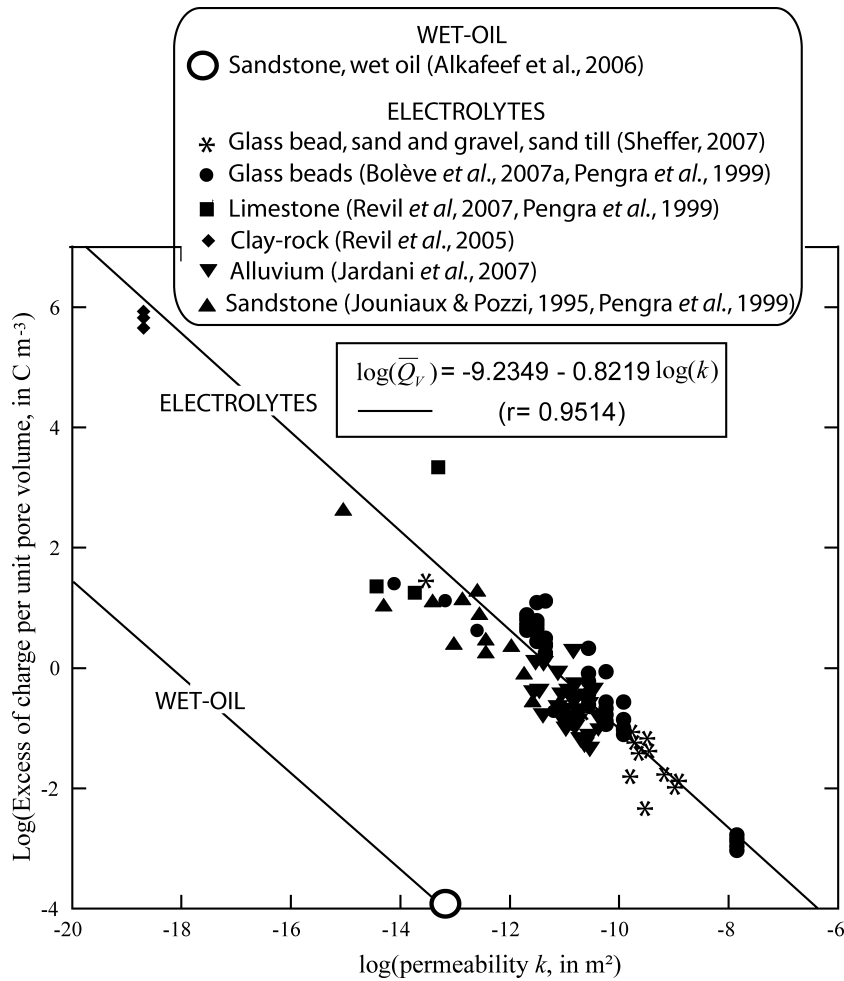


**Figure 3.** Bulk charge density of the diffuse layer per unit pore volume of the rock as a function of the DC-permeability  $k_0$ . The experimental data are from different types of rocks and the pH of the electrolytes is comprised between 6 and 9. Experimental data from Jouniaux & Pozzi (1995), Pengra *et al.* (1999), Revil *et al.* (2005), Bolève *et al.* (2007), Revil *et al.* (2007), Sheffer (2007) and Jardani *et al.* (2007). For porous materials filled with wet-oil, we expect that a similar trend occurs but the volumetric charge density in the pore space would be smaller by comparison with an electrolyte-filled porous medium having the same permeability.

where  $F$  is the electrical formation factor defined by the ratio between the tortuosity and the porosity,  $\Sigma_S$  is the specific surface conductivity associated with the electromigration of charge carriers (counterions and protons) in the electrical double layer,  $\bar{\sigma}_f$  is the effective conductivity of the pore fluid including the effect of the electrical diffuse layer as discussed by Revil & Leroy (2004) and Revil *et al.* (2005) and  $\Lambda$  is the characteristic pore size defined by Johnson (1986). A model of  $\Sigma_S$  including the contribution of the Stern layer has been developed recently by Leroy *et al.* (2008) for aqueous solutions and can be used to assess the frequency dependence of this parameter. For simplicity, however, we assume that  $\Sigma_S$ , and hence conductivity, are independent of frequency in the developments that follow.

The generalized Darcy's and Ohm's laws appear therefore as cross-coupled constitutive equations

$$\begin{bmatrix} -i\omega\bar{\mathbf{w}} \\ \mathbf{j} \end{bmatrix} = \begin{bmatrix} \frac{k(\omega)}{\eta_f} & -c(\omega)\sigma \\ -c(\omega)\sigma & \sigma \left( 1 + \frac{c(\omega)^2\eta_f\sigma}{k(\omega)} \right) \end{bmatrix} \times \begin{bmatrix} -\nabla\bar{p}_f + \rho_f\omega^2\bar{\mathbf{u}}_s + \bar{\mathbf{F}}_f \\ \mathbf{E} \end{bmatrix}, \quad (41)$$

where  $\bar{\mathbf{F}}_f$  is the applied body-force acting on the fluid phase.

The normalized dynamic permeability is given by

$$\tilde{k}(\omega) \equiv \frac{k(\omega)}{k_0} = \frac{1 - (i\omega\tau_m)^c}{1 - i(\omega/\omega_c)[1 - (i\omega\tau_m)^c]}, \quad (42)$$

where  $k_0 = \Lambda^2/(8F)$  (Johnson 1986) is the permeability at low frequencies  $\omega \ll \text{Min}(\omega_c, \omega_m)$ ,  $\omega_m = 1/\tau_m$  and  $\omega_c = \eta_f/(k_0\rho_f F)$ . Both  $F$  and  $\Lambda$  are two textural parameters defined by (Johnson 1986)

$$\frac{1}{F} = \frac{1}{V} \int_{V_p} \mathbf{e}^2 dV_p, \quad (43)$$

$$\Lambda = 2 \frac{\int_{V_p} \mathbf{e}^2 dV_p}{\int_S \mathbf{e}^2 dS}, \quad (44)$$

where  $dV_p$  denotes an integration over the pore space and  $dS$  denotes an integration over the pore–solid interface. The normalized electrical field  $\mathbf{e} = \nabla\Gamma$  is obtained by solving the following canonical Laplace problem for an average disc in the direction of the macroscopic electrical field (see Pride 1994):  $\Gamma$  has units of length,  $\Gamma$  satisfies Laplace equation  $\nabla^2\Gamma = 0$  throughout the pore space with boundary conditions  $\Gamma = 0$  on  $z = 0$  and  $\Gamma = L$  on  $z = L$ , and  $\hat{\mathbf{n}} \cdot \nabla\Gamma = 0$  on both the internal interface between the solid and fluid phases ( $\hat{\mathbf{n}}$  is the unit vector at the solid–fluid interface pointing

inside the solid) and on the external surface of the averaging disc ( $\hat{\mathbf{n}}$  is the outward unit vector). This approach assumed implicitly the continuity of the solid phase at the scale of a representative elementary volume of the porous rock.

The dynamic streaming potential coupling coefficient is given by

$$c(\omega) = -\frac{\bar{Q}_V k(\omega)}{\eta_f \sigma}. \quad (45)$$

The normalized coupling coefficient is given by

$$\tilde{c}(\omega) \equiv \frac{c(\omega)}{c_0} = \tilde{k}(\omega). \quad (46)$$

Therefore, in our approach, the normalized dynamic coupling coefficient is equal to the normalized dynamic permeability, the normalization being made with respect to the DC value of these parameters.

Using the thin double layer assumption and the Boltzmann distribution for the concentrations in the diffuse layer (small size of the diffuse layer with respect to the size of the pores), the dynamic relative coupling coefficient of a porous material saturated by a viscous Newtonian fluid is given by (Pride 1994)

$$\tilde{c}(\omega) = \frac{1}{\sqrt{1 - 2i\omega/\omega_c}}, \quad (47)$$

and  $c_0 = \varepsilon_f \zeta / (\eta_f \sigma_f)$  (Helmholtz–Smoluchowski equation) where  $\zeta$  is the so-called zeta potential (the inner potential of the electrical diffuse layer).

Using the dynamic viscosity defined by eq. (16) and using eq. (47), the dynamic relative coupling coefficient of a porous material saturated by a generalized Maxwell fluid in the thin double layer assumption is given by

$$\tilde{c}(\omega) = \frac{1 - (i\omega\tau_m)^c}{\sqrt{1 - 2i(\omega/\omega_c)[1 - (i\omega\tau_m)^c]}}. \quad (48)$$

In eq. (48), the effect of the viscosity appears twice: in the numerator because of the dependence of  $c_0$  with the viscosity and in the last term in the denominator because of the dependence of the critical frequency  $\omega_c$  with the viscosity. It is interesting to see that eq. (48) has the same asymptotic limit at low frequencies as eqs (42) and (46) using the Donnan assumption. This limit is given by  $1 + i(\omega/\omega_c)$  for a Newtonian fluid.

The excitation of the pore fluid in the resonance frequency band of the viscoelastic fluid yields an amplification of the value of the streaming potential coupling coefficient by several orders of magnitude with respect to the value of the streaming potential coupling coefficient at low frequencies. We expect that the determination of  $\tilde{c}(\omega)$  in a wide range of frequencies (e.g. 0.01–10 kHz in the laboratory) could help to characterize the properties of the oil contained in the pores through the determination of both  $\tau_m$ , the peak of the relaxation time, and the exponent  $c$ , which characterizes the broadness of the distribution of the relaxation times associated with the composition of the oil in terms of polymers.

We can determine also an order of magnitude of the DC-value of the streaming potential coupling coefficient of a sandstone filled with a polar oil. For the Berea sandstone (permeability  $\sim 10^{-13}$  m<sup>2</sup>, porosity  $\sim 0.18$ ), an analysis of the data displayed by Alkafef *et al.* (2006) for the streaming current density versus the fluid pressure gradient yields  $\bar{Q}_V = 10^{-4}$  C m<sup>-3</sup>. Alkafef *et al.* (2006) used a crude oil containing asphaltene, a strongly polar polymer responsible for a high dielectric constant for this fluid. The previous analysis implies a charge density 6 orders of magnitude smaller than existing in a sandstone of same permeability filled by an electrolyte (Fig. 3).

The shear viscosity of the crude oil is equal to  $5 \times 10^{-3}$  Pa s at 25 °C (Alkafef *et al.* (2006)). Using  $\sigma = 2 \times 10^{-10}$  S m<sup>-1</sup>, we find a streaming potential coupling coefficient on the order of  $c_0 = -4 \times 10^{-5}$  V Pa<sup>-1</sup>. So the low value of the charge density is more than compensated by the effect of the high value of the electrical resistivity of the fluid. Indeed,  $-4 \times 10^{-5}$  V Pa<sup>-1</sup> is a very high value by comparison with the value of the streaming potential coupling coefficient of a typical soil or reservoir rock saturated by a brine (typically in the range from  $-(10^{-6}$  to  $10^{-8})$  V Pa<sup>-1</sup>, see Revil *et al.* 2003). This implies than even much below the relaxation frequency of the resonance of the solvent, the streaming potential coupling coefficient of a sandstone filled with such an oil can reach a very large value.

#### 4 THE MECHANICAL EQUATIONS

The bulk stress tensor is defined by

$$\bar{\mathbf{T}} = (1 - \phi)\bar{\mathbf{T}}_s + \phi\bar{\mathbf{T}}_f. \quad (49)$$

where  $\bar{\mathbf{T}}_s$  and  $\bar{\mathbf{T}}_f$  are the phase average stress tensors in the solid phase and viscoelastic fluid, respectively. The confining pressure and the deviatoric stress of the porous body are defined by

$$P \equiv -tr(\bar{\mathbf{T}})/3 = (1 - \phi)\bar{p}_s + \phi\bar{p}_f, \quad (50)$$

$$\bar{\mathbf{T}}^D \equiv \bar{\mathbf{T}} + P\mathbf{I}, \quad (51)$$

where  $\bar{p}_s$  is the mean pressure in the solid phase. The deviatoric stress is then given by

$$\bar{\mathbf{T}}^D = (1 - \phi)\bar{\mathbf{T}}_s^D + \phi\bar{\boldsymbol{\pi}}, \quad (52)$$

where  $\bar{\mathbf{T}}_s^D = \bar{\mathbf{T}}_s + \bar{p}_s\mathbf{I}$  is the mean deviatoric stress of the solid phase and  $\bar{\boldsymbol{\pi}}$  is the mean deviatoric stress in the pore fluid phase (see Appendix A).

Performing a volume-average of the force balance equations in each phase, eqs (17) and (25), yield a total force balance equation in the time domain

$$(1 - \phi)\nabla \cdot \bar{\mathbf{T}}_s + \phi\nabla \cdot \bar{\mathbf{T}}_f + \mathbf{F} = (1 - \phi)\rho_s\ddot{\mathbf{u}}_s + \phi\rho_f\ddot{\mathbf{u}}_f, \quad (53)$$

$$\nabla \cdot \bar{\mathbf{T}} + \mathbf{F} = \rho\ddot{\mathbf{u}}_s + \rho_f\ddot{\mathbf{w}}, \quad (54)$$

where the bulk density and the bulk force are defined by

$$\rho = \phi\rho_f + (1 - \phi)\rho_s, \quad (55)$$

$$\mathbf{F} = (1 - \phi)\bar{\mathbf{F}}_s + \phi\bar{\mathbf{F}}_f, \quad (56)$$

respectively. An expression of the force in terms of source mechanism will be given in Section 6.4.

The total stress tensor and the pore fluid pressure are given by (see Appendix A)

$$\bar{\mathbf{T}} = K_U(\nabla \cdot \bar{\mathbf{u}}_s)\mathbf{I} + C(\nabla \cdot \bar{\mathbf{w}})\mathbf{I} + 2G_U \otimes \bar{\mathbf{d}}_s + 2C_G \otimes \bar{\mathbf{d}}_w, \quad (57)$$

$$\bar{\mathbf{T}}_f = C(\nabla \cdot \bar{\mathbf{u}}_s)\mathbf{I} + M(\nabla \cdot \bar{\mathbf{w}})\mathbf{I} + 2C_G \otimes \bar{\mathbf{d}}_s + 2M_G \otimes \bar{\mathbf{d}}_w, \quad (58)$$

where the circled cross stands for the Stieltjes convolution product,  $K_U$  and  $G_U$  are the undrained bulk and shear moduli of the porous medium, and  $C$  and  $M$  are two Biot moduli.

5 THE MAXWELL EQUATIONS

As shown by Pride (1994), the local Maxwell equations can be volume-averaged to obtain the macroscopic Maxwell equations (see also Revil & Linde 2006, who used the Donnan model discussed in Section 3). With the Donnan model, the Maxwell equations are

$$\nabla \times \mathbf{E} = -\dot{\mathbf{B}}, \tag{59}$$

$$\nabla \times \mathbf{H} = \mathbf{j} + \dot{\mathbf{D}}, \tag{60}$$

$$\nabla \cdot \mathbf{B} = 0, \tag{61}$$

$$\nabla \cdot \mathbf{D} = \phi \bar{Q}_V, \tag{62}$$

where  $\mathbf{H}$  is the magnetic field,  $\mathbf{B}$  is the magnetic induction and  $\mathbf{D}$  is the displacement vector. These equations are completed by two electromagnetic constitutive equations:  $\mathbf{D} = \varepsilon \mathbf{E}$  and  $\mathbf{B} = \mu \mathbf{H}$  where  $\varepsilon$  is the permittivity of the medium and  $\mu$  is the magnetic permeability. If the porous material does not contain magnetized grains, these two material properties are given by (Pride 1994)

$$\varepsilon = \frac{1}{F} [\varepsilon_f + (F - 1)\varepsilon_s], \tag{63}$$

$$\mu = \mu_0, \tag{64}$$

where  $F$  is the electrical formation factor defined by eq. (43),  $\varepsilon_f$  and  $\varepsilon_s$  are the dielectric constants of the pore fluid and the solid, respectively, and  $\mu_0$  is the magnetic permeability of free space. Note that only two textural properties  $\Lambda$  and  $F$  are required to describe the influence of the topology of the pore network upon the material properties entering the transport and electromagnetic constitutive equations.

The coupling between the mechanical and the Maxwell equations occurs in the current density, which can be written in the time domain as

$$\mathbf{j} = \sigma \mathbf{E} + \mathbf{j}_S, \tag{65}$$

$$\mathbf{j}_S = \bar{Q}_V \dot{\mathbf{w}} = -\frac{k(\omega)\bar{Q}_V}{\eta_f} (\nabla \bar{p}_f + \rho_f \ddot{\mathbf{u}}_s - \bar{\mathbf{F}}_f), \tag{66}$$

where  $\mathbf{j}_S$  is the source current density of electrokinetic nature. The body force  $\bar{\mathbf{F}}_f$  can be responsible for electromagnetic signals that are directly associated with the source.

6 IMPLEMENTATION OF THE FIELD EQUATIONS

6.1 Field equations

In this section, we are interested to solve the seismoelectric problem for poroelastic media saturated by Newtonian or generalized viscoelastic fluids. As the case of a poroelastic body saturated by a Newtonian fluid is a special case of the theory develop above, we develop the general field equations below and we show that these equations yields the correct estimates in the limit of a Newtonian fluid.

For the seismoelectric problem and neglecting the electrosmotic contribution in the Darcy velocity, the three equations to solve are given, in the time domain, by Darcy's law plus combined equations of motion for the solid and the fluid phases,

$$b(t) \otimes \dot{\mathbf{w}} + \tilde{\rho}_f \ddot{\mathbf{w}} = -(\nabla \bar{p}_f + \rho_f \ddot{\mathbf{u}}_s - \bar{\mathbf{F}}_f), \tag{67}$$

$$\rho \ddot{\mathbf{u}}_s + \rho_f \ddot{\mathbf{w}} - \nabla \cdot \bar{\mathbf{T}} = \mathbf{F}, \tag{68}$$

$$\frac{\bar{p}_f}{M} + \nabla \cdot \bar{\mathbf{w}} + \alpha \nabla \cdot \ddot{\mathbf{u}}_s = 0, \tag{69}$$

where  $M$  is one of the Biot' moduli (see Appendix A). eq. (67) is derived from eq. (41) in Appendix B,  $b(t) = \eta_f^*(t)/k_0$  is defined in Appendix C,  $\eta_f^*(t)$  is the inverse Fourier transform of  $\eta_f^*(\omega)$  defined by eq. (16),  $\tilde{\rho}_f$  is defined by eq. (B3). Eq. (68) follows from eq. (54) while eq. (69) follows from eq. (A41) using the relationship  $\alpha = C/M$ .

Taking the time derivative of eq. (69) and using Darcy's law in which we have neglected the electrosmotic contribution (the last term of eq. 38) because we are only interested in this paper by the seimoelectric coupling, we obtain, in the frequency domain, the following hydraulic diffusion equation for the pore water (see Appendix B)

$$\frac{-i\omega \bar{p}_f}{M} + \nabla \cdot \left[ \frac{k(\omega)}{\eta_f} (-\nabla \bar{p}_f + \omega^2 \rho_f \ddot{\mathbf{u}}_s) \right] = \alpha \nabla \cdot (i\omega \ddot{\mathbf{u}}_s). \tag{70}$$

The assumption that the electrosmotic component can be neglected if we are dealing with the electromagnetic field associated with hydromechanical disturbances has been investigated by Revil *et al.* (1999) among others. The first term of the left-hand-side of eq. (70) corresponds to the storage term while the second term corresponds to the divergence of the Darcy velocity. The term on the right-hand side of eq. (70) corresponds to a source term for this PDE.

For a 2-D problem, eqs (67) and (68) can be combined to give (see Appendix B)

$$\nabla \cdot \bar{\bar{\Gamma}} = \bar{\bar{F}}, \tag{71}$$

$$\bar{\bar{\Gamma}} \equiv \begin{bmatrix} T_{xx} & T_{xz} \\ T_{zx} & T_{zz} \\ -\bar{p}_f & 0 \\ 0 & -\bar{p}_f \end{bmatrix}, \tag{72}$$

$$\bar{\bar{F}} \equiv \begin{bmatrix} -F_x + \rho \ddot{u}_x + \rho_f \ddot{w}_x \\ -F_z + \rho_f \ddot{u}_z + \rho_f \ddot{w}_z \\ \rho_f \ddot{u}_x + \tilde{\rho}_f \ddot{w}_x \\ \rho_f \ddot{u}_z + \tilde{\rho}_f \ddot{w}_z \end{bmatrix}, \tag{73}$$

where  $\bar{p}_f$  is related directly to the components of the displacement of the solid and the components of  $\bar{\mathbf{w}}$  by eq. (69). This form is suitable for the implementation into a finite element code. We use Comsol Multiphysics 3.4 adding perfect matched layer (PML) boundary conditions to the problem for the poroelastic waves and associated electrical signals (see Zeng *et al.* 2001; Jardani *et al.* 2010). This is to avoid spurious reflections at the side and bottom boundaries of the system. eq. (71) is solved first for the poroelastic propagation problem, which gives the solution for the unknown variables ( $u_x, u_z, w_x, w_z$ ).

The electromagnetic problem is solved in the quasi-static limit. To simplify the problem, we consider that the reservoir is close enough from the sensors (antennas, non-polarizing electrodes and/or magnetometers). In this case, we can neglect the time required by the electromagnetic disturbances to diffuse between the reservoir and the electromagnetic sensors. With this additional assumption, we can model the problem by solving only the quasi-static electromagnetic problem (rather than the low-frequency diffusive problem) for the electrical potential and the magnetic fields

$$\nabla \cdot (\sigma \nabla \psi) = \nabla \cdot \mathbf{j}_S, \tag{74}$$

$$\nabla^2 \mathbf{B} = -\mu_0 \nabla \times \mathbf{j}_S, \quad (75)$$

where  $\psi$  is the electrostatic potential ( $\mathbf{E} = -\nabla\psi$  in the quasi-static limit of the Maxwell equations), and  $\mathbf{j}_S = \bar{Q}_V \dot{\mathbf{w}}$ .

## 6.2 Dilatational wave speeds

Combining eqs (69) and (70) yields

$$\left(\rho - \frac{\rho_f}{F}\right) \ddot{\mathbf{u}}_s = \nabla \cdot \bar{\mathbf{T}} - \frac{1}{F} \nabla \cdot \bar{\mathbf{T}}_f + \frac{b(t)}{F} \otimes \dot{\mathbf{w}}, \quad (76)$$

$$\left(F - \frac{\rho_f}{\rho}\right) \rho_f \ddot{\mathbf{w}} = \nabla \cdot \bar{\mathbf{T}}_f - \frac{\rho_f}{\rho} \nabla \cdot \bar{\mathbf{T}} - \frac{b(t)}{F} \otimes \dot{\mathbf{w}}. \quad (77)$$

These two equations have the same structure as eqs (183) and (184) of Morency & Tromp (2008). As shown in Appendix C, the frequency or time dependence of the material properties is however quite different. While Morency & Tromp (2008) investigated dissipation mechanisms associated with the behaviour of the skeleton in terms of an equivalent viscoelastic behaviour of the material, the dissipation mechanism occurring in our model is stemming from the viscoelastic properties of the pore fluid.

In the time domain, the constitutive equations for the total stress tensor and the fluid phase average stress tensor are given in Appendix A

$$\bar{\mathbf{T}} = K_U (\nabla \cdot \bar{\mathbf{u}}_s) \mathbf{I} + C (\nabla \cdot \bar{\mathbf{w}}) \mathbf{I} + 2G_U(t) \otimes \bar{\mathbf{d}}_s + 2C_G(t) \otimes \bar{\mathbf{d}}_w, \quad (78)$$

$$\bar{\mathbf{T}}_f = C (\nabla \cdot \bar{\mathbf{u}}_s) \mathbf{I} + M (\nabla \cdot \bar{\mathbf{w}}) \mathbf{I} + 2C_G(t) \otimes \bar{\mathbf{d}}_s + 2M_G(t) \otimes \bar{\mathbf{d}}_w, \quad (79)$$

$$G_U(t) = \text{FT}^{-1} G_U(\omega), \quad (80)$$

$$C_G(t) = \text{FT}^{-1} C_G(\omega), \quad (81)$$

$$M_G(t) = \text{FT}^{-1} M_G(\omega), \quad (82)$$

where the deviators  $\bar{\mathbf{d}}_s$  and  $\bar{\mathbf{d}}_w$  are defined in Appendix A and  $\bar{\mathbf{d}}$  is the mean strain deviator of the solid phase, and the coefficients  $G_U(t)$ ,  $G_U(\omega)$ ,  $C_G(t)$ ,  $C_G(\omega)$ ,  $M_G(t)$  and  $M_G(\omega)$  are defined in Appendix A.

We use the classical decomposition of the displacements into dilatational components

$$\nabla \cdot \bar{\mathbf{u}}_s = e, \quad (83)$$

$$\nabla \cdot \bar{\mathbf{w}} = \zeta. \quad (84)$$

The dilatational wave propagation is obtained by applying the divergence operator to eqs (76) and (77) substituting eqs (78) and (79). This yields

$$\left(\rho - \frac{\rho_f}{F}\right) \ddot{e} \nabla^2 [H \otimes e + C\zeta] - \frac{1}{F} \nabla^2 (Ce + M\zeta) + \frac{b(t)}{F} \otimes \dot{\zeta}, \quad (85)$$

$$\left(F - \frac{\rho_f}{\rho}\right) \rho_f \ddot{\zeta} = \nabla^2 [Ce + M\zeta] - \frac{\rho_f}{\rho} \nabla^2 (H \otimes e + C\zeta) - b(t) \otimes \dot{\zeta}, \quad (86)$$

where  $H$  is the stiffness coefficient of Biot theory ( $H = K_U + (4/3)G_U$ ). We assume plane wave propagation in the  $x$ -direction

$$e = A_1 \exp[i(lx - \omega t)], \quad (87)$$

$$\zeta = A_2 \exp[i(lx - \omega t)], \quad (88)$$

where  $\omega$  is the angular frequency,  $l$  is the complex wavenumber, and  $z_p = \omega/l$  is the complex speed. Using eqs (87) and (88) into (85) and (86), we obtain

$$\left(\rho - \frac{\rho_f}{F}\right) (-\omega^2 A_1) = H(\omega)(-A_1 l^2) - C A_2 l^2 + \frac{1}{F} (C A_1 l^2 + M A_2 l^2) - i\omega \frac{b(\omega)}{F} A_2, \quad (89)$$

$$\left(F - \frac{\rho_f}{\rho}\right) \rho_f (-\omega^2 A_2) = -C l^2 A_1 - M l^2 A_2 + \frac{\rho_f}{\rho} (H(\omega) l^2 A_1 + C l^2 A_2) + i\omega A_2 b(\omega). \quad (90)$$

Eliminating  $A_1$  and  $A_2$  between these two equations yields the following equation for the speed:  $az_p^4 + bz_p^2 + c = 0$ , with

$$a = \rho - \frac{\rho_f}{F} + i \frac{b(\omega)}{\omega} \left(\frac{\rho}{\bar{\rho}_f}\right), \quad (91)$$

$$b = (-1) \left[ \frac{M\rho}{\bar{\rho}_f} + H(\omega) - \frac{2C}{F} + i \frac{b(\omega)}{\omega \bar{\rho}_f} H(\omega) \right], \quad (92)$$

$$c = \frac{1}{\bar{\rho}_f} [H(\omega)M - C^2]. \quad (93)$$

The two roots of this equation are

$$(z_p^I)^2 = \frac{-b + \sqrt{b^2 - 4ac}}{2a}, \quad (94)$$

$$(z_p^{II})^2 = \frac{-b - \sqrt{b^2 - 4ac}}{2a}, \quad (95)$$

with  $z_p^I > z_p^{II}$ . These two waves correspond to the complex wave speeds associated with the fast  $P$  wave when the solid and the fluid move in phase and the slow dilatational (slow) wave when the solid and the fluid move out of phase. The phase speeds are given by  $1/c_p^I = \text{Re}[(z_p^I)^{-1}]$  and  $1/c_p^{II} = \text{Re}[(z_p^{II})^{-1}]$  and the inverse quality factors are  $1/Q_p^I = \text{Im}(z_p^I)^2 / \text{Re}(z_p^I)^2$  and  $1/Q_p^{II} = \text{Im}(z_p^{II})^2 / \text{Re}(z_p^{II})^2$ .

## 6.3 Rotational wave speeds

Using the decomposition of the displacements into rotational components

$$\nabla \times \bar{\mathbf{u}}_s = \boldsymbol{\Omega}, \quad (96)$$

$$\nabla \times \bar{\mathbf{w}} = \boldsymbol{\Psi}, \quad (97)$$

applying the curl operator to eqs (76) and (77), and using eqs (78) and (79), we obtain

$$\left(\rho - \frac{\rho_f}{F}\right) \ddot{\boldsymbol{\Omega}} = G_U \otimes \nabla^2 \boldsymbol{\Omega} + C_G \otimes \nabla^2 \boldsymbol{\Psi} - \frac{1}{F} C_G \otimes \nabla^2 \boldsymbol{\Omega} - \frac{1}{F} M_G \otimes \nabla^2 \boldsymbol{\Psi} + \frac{b(t)}{F} \otimes \dot{\boldsymbol{\Psi}}, \quad (98)$$

$$\left(F - \frac{\rho_f}{\rho}\right) \rho_f \ddot{\Psi} = C_G \otimes \nabla^2 \Omega + M_G \otimes \nabla^2 \Psi - \frac{\rho_f}{\rho} G_U \otimes \nabla^2 \Omega - \frac{\rho_f}{\rho} C_G \otimes \nabla^2 \Psi - b(t) \otimes \dot{\Psi}. \quad (99)$$

We assume plane wave propagation in the  $x$ -direction

$$\Omega = B_1 \exp[i(lx - \omega t)], \quad (100)$$

$$\Psi = B_2 \exp[i(lx - \omega t)], \quad (101)$$

where  $\omega$  is the angular frequency,  $l$  is the complex wavenumber, and  $z_S = \omega/l$  is the complex speed. Using these equations, we obtain

$$\left(\rho - \frac{\rho_f}{F}\right) (-\omega^2 B_1) = G_U(\omega) (-B_1 l^2) - C_G B_2 l^2 + \frac{1}{F} (C_G B_1 l^2 + M_G B_2 l^2) - i\omega \frac{b(\omega)}{F} B_2, \quad (102)$$

$$\left(F - \frac{\rho_f}{\rho}\right) \rho_f (-\omega^2 B_2) = -C_G l^2 B_1 - M_G l^2 B_2 + \frac{\rho_f}{\rho} (G_U l^2 B_1 + C_G l^2 B_2) + i\omega B_2 b(\omega). \quad (103)$$

Eliminating  $B_1$  and  $B_2$  between these two equations yields the following equation for the speed:  $a' z_S^4 + b' z_S^2 + c' = 0$ , with

$$a' = \rho - \frac{\rho_f}{F} + i \frac{b(\omega)}{\omega} \left(\frac{\rho}{\tilde{\rho}_f}\right), \quad (104)$$

$$b' = (-1) \left[ \frac{M_G(\omega)\rho}{\tilde{\rho}_f} + G_U(\omega) - \frac{2C_G(\omega)}{F} + i \frac{b(\omega)}{\omega \tilde{\rho}_f} G_U(\omega) \right], \quad (105)$$

$$c' = \frac{1}{\tilde{\rho}_f} [G_U(\omega)M_G(\omega) - C_G(\omega)^2]. \quad (106)$$

The two roots of this equation are

$$(z_S^I)^2 = \frac{-b' + \sqrt{b'^2 - 4a'c'}}{2a'}, \quad (107)$$

$$(z_S^{II})^2 = \frac{-b' - \sqrt{b'^2 - 4a'c'}}{2a'}, \quad (108)$$

with  $z_S^I > z_S^{II}$ . These two waves correspond to the complex wave speeds associated with a fast rotational  $S$  wave and a slow rotational  $S$  wave. The slow rotational wave represents the classical shear wave while the fast rotational wave is related to the fact that the fluid can sustain shear stresses above its resonance frequency. This wave does not exist at low frequencies ( $\omega \ll \omega_m$ ) because the pore fluid behaves as a Newtonian fluid. The phase speeds of these two waves are given by  $1/c_S^I = \text{Re}[(z_S^I)^{-1}]$  and  $1/c_S^{II} = \text{Re}[(z_S^{II})^{-1}]$  and the inverse quality factors are  $1/Q_S^I = \text{Im}(z_S^I)^2 / \text{Re}(z_S^I)^2$  and  $1/Q_S^{II} = \text{Im}(z_S^{II})^2 / \text{Re}(z_S^{II})^2$ , respectively.

To check the consistency of the model, we can look for the case where  $G_f^*(\omega) = 0$  and  $G_U = G_{fr}$ ,  $C_G(\omega) = 0$ , and  $M_G(\omega) = 0$ . In this case, we obtain

$$a' = \rho - \frac{\rho_f}{F} + i \frac{b(\omega)}{\omega} \left(\frac{\rho}{\tilde{\rho}_f}\right), \quad (109)$$

$$b' = -G_{fr} \left[ 1 + i \frac{b(\omega)}{\omega \tilde{\rho}_f} \right], \quad (110)$$

$$c' = 0, \quad (111)$$

and therefore

$$(z_S^I)^2 = 0, \quad (112)$$

$$(z_S^{II})^2 = G_{fr} \left(\frac{\tilde{\rho}_f}{\rho}\right) \frac{\tilde{\rho}_f - \frac{\rho_f^2}{\rho} + \frac{b^2(\omega)}{\omega^2 \tilde{\rho}_f} - i \frac{b(\omega)}{\omega} \frac{\rho_f}{F\rho}}{\left(\tilde{\rho}_f - \frac{\rho_f^2}{\rho}\right)^2 + \left[\frac{b(\omega)}{\omega}\right]^2}. \quad (113)$$

In absence of dissipation, this second wave corresponds to the classical shear wave with phase speed

$$c_S^2 = \frac{G_{fr}}{\rho - \rho_f/F}, \quad (114)$$

(see Morency & Tromp 2008).

## 6.4 Mechanical source

The macroscopic source term  $\mathbf{F}$  is linearly partitioned between the solid and the fluid phases, see eq. (56). It can be written in terms of the moment tensor  $\mathbf{M}$  by (Dahlen & Tromp 1998)

$$\mathbf{F} = -\mathbf{M} \cdot \nabla \delta(\mathbf{x} - \mathbf{x}_S) S(t), \quad (115)$$

where  $\mathbf{x}_S$  refers to the position of the source,  $S(t)$  is the source–time function, and  $\delta(\mathbf{x})$  is the Dirac (delta) function. This source term arises in eq. (71) to determine the initial values of the displacements of the solid phase and the relative displacement of the fluid phase with respect to the solid. Then the relative displacement of the fluid phase with respect to the solid phase creates a source term in the electrostatic and magnetostatic field equations, eqs (74) and (75).

## 7 SYNTHETIC CASE STUDIES

Experiment #1 corresponds to the simulation of the seismoelectric response of an oil-filled reservoir (see Fig. 4) in an half-space with the oil considered as a Newtonian fluid. The ground surface corresponds to the top surface of the system where the normal component of the electrical field vanishes. The material properties of the embedding medium (with the properties of a sandstone) and the oil reservoir are reported in Table 1. We consider a volumetric source located 50 m below the ground surface generating  $P$  waves. The reservoir is 100 m thick and its top surface is located 250 m below the ground surface (Fig. 4a). The time dependence of the source  $S(t)$  is a Ricker with a dominant frequency of 30 Hz. We consider the arrival of the seismic and seismoelectric signals at a station  $P_1(-50 \text{ m}, 0 \text{ m})$  corresponding to a single electrode. The reference for the electrical potential recorded at this electrode is located at position  $\text{Ref}(-300 \text{ m}, 0 \text{ m})$  (see Fig. 4). The four edges are absorbing boundaries for which we use PML boundary conditions (see Jardani *et al.* 2010 for more details). To solve numerically the problem, we use the finite element modelling Comsol Multiphysics 3.5 to simulate both seismograms and electrograms at the ground surface.

Both seismoelectric conversion and coseismic electrical signals are generated at the reservoir boundaries (Figs 4b, 5 and 6). Fig. 6 shows two electrograms for station  $P_1$ . The first type of signals corresponds to the co-seismic electrical signal associated with the propagation of the  $P$  wave. It is labelled ‘Coseismic’ in Figs 5(a) and 6. Other coseismic signals are associated with the reflected  $P$  waves at the top and bottom interfaces of the reservoir. These coseismic signals are labelled RCS1 and RCS2, respectively. These coseismic

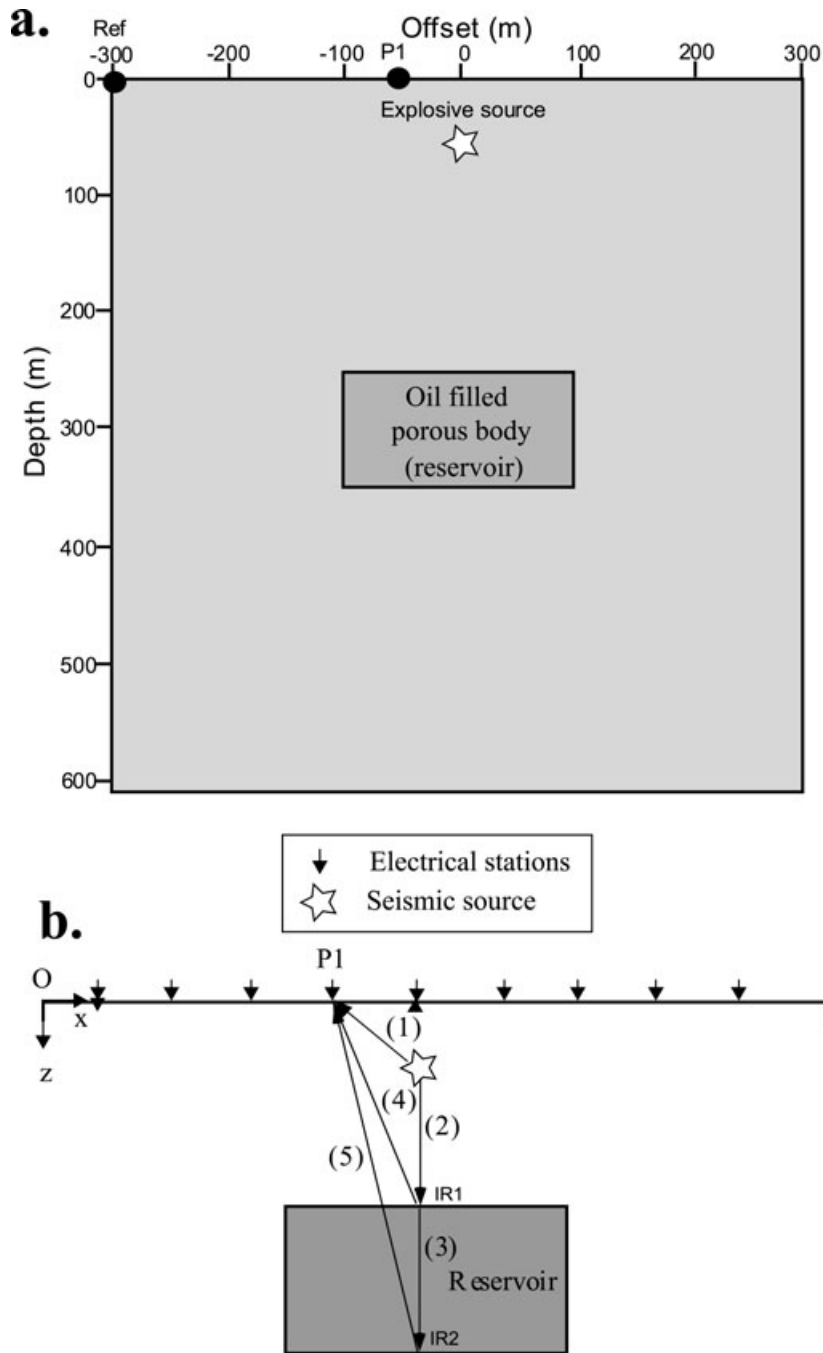


**Figure 4.** The depth of the oil reservoir is 250 m. Its length and thickness are 200 and 100 m, respectively. The depth of the source is 50 m. The observation station is  $P_1$ . There is a signal associated with the source itself that diffuses nearly instantaneously at the observation station. We decided not to model this signal. In the early times of the electrogram, various contributions include the seismoelectric conversions of the  $P$  wave reaching the top of the reservoir (2) (labelled IR1) and the bottom of the reservoir (3) (labelled IR2). In addition, coseismic signals are associated with the direct wave (1) (labelled 'coseismic') and the reflected waves (4) and (5) (labelled RCS1 and RCS 2).

signals occur when a seismic wave travels through a porous material, creating a relative displacement between the pore water and the solid phase. The associated current density is balanced by a conduction current density. It results an electrical field travelling at the same speed as the seismic wave. The second type of seismoelectric signals correspond to converted seismoelectric signals associated with the arrival of the  $P$  waves at the top and bottom interface of the oil reservoir. These converted seismoelectric signals are labelled IR1 and IR2, respectively. When crossing an interface between

two domains characterized by different properties, a seismic wave generates a time-varying charge separation, which acts as a dipole radiating electromagnetic energy. These dipoles oscillate with the waveform of the seismic waves. Because the electromagnetic diffusion of the electrical disturbance is very fast (instantaneous in our simulations), the seismoelectric conversions are observed nearly at the same time by all the electrodes but with different amplitudes. The seismoelectric conversions appear therefore as flat lines in the electrograms shown in Fig. 5(a).

**Table 1.** Properties of reservoir for the second numerical experiment (Experiment #2).

Parameter	Embedding medium	Reservoir
$K_s$	35 GPa	37 GPa
$K_{fr}$	5.00 GPa	1.07 GPa
$K_f$	0.225 GPa	2.4 GPa
$G$	4 GPa	5 GPa
$\eta_f$	$10^{-3}$ Pa s	0.8 Pa s
$k_0$	$10^{-14}$ m <sup>2</sup>	$10^{-12}$ m <sup>2</sup>
$\sigma$	0.01 S m <sup>-1</sup>	$10^{-4}$ S m <sup>-1</sup>
$\bar{Q}_V$	10 C m <sup>-3</sup>	1000 C m <sup>-3</sup>
$\phi$	0.25	0.335

Experiment #2 uses the same geometry as Experiment #1 but the fluid in the reservoir is now a viscoelastic wet-oil. The dynamic permeability response of the reservoir filled with the viscoelastic fluid is shown in Fig. 7(a). The time function of the source is a Dirac and we investigate the electrical field response in the frequency band (1–1000 Hz). A plot of the vertical component of the electrical field at an observation point at depth is shown in Fig. 7(b). The maximum of the electrical field occurs at the same frequency that the resonance of the viscoelastic fluid. The amplification of the electrical field reaches several orders of magnitude with respect to the DC-value. This very strong amplification of the signal could be the basis of a new detection and mapping method of heavy oils and DNAPL in the ground.

## 8 CONCLUDING STATEMENTS

We have developed a model to simulate the seismoelectric coupling in a poroelastic body saturated by a viscoelastic or a Newtonian fluid ignoring the electroosmotic term in the Darcy equation and assuming that the electromagnetic disturbances generated by the seismoelectric conversions move instantaneously through the conductive Earth. The following conclusions are reached.

(1) When the pore fluid is a wet oil, it can be also considered as a viscoelastic non-aqueous solvent with a finite electrical conductivity and a relatively high dielectric constant (but always lower than the dielectric constant of water).

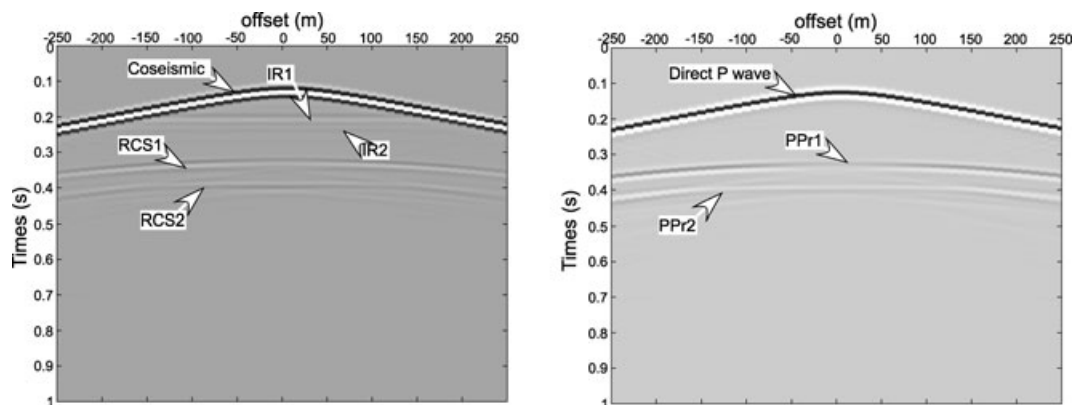


**Figure 5.** Electrograms and sismograms. (a) The electrograms show the coseismic electrical potential field associated with the direct wave and with the reflections of the  $P$  wave (labelled RCS1 and RCS 2) and the seismoelectric conversions with a smaller amplitude and a flat shape (labelled IR1 and IR2). (b) The sismograms reconstructed by the geophones show the  $P$ -wave direct field and the reflections of the  $P$  waves. The reflections PPr1 and PPr2 correspond to the re-reflections on the top and bottom of the reservoir, respectively.

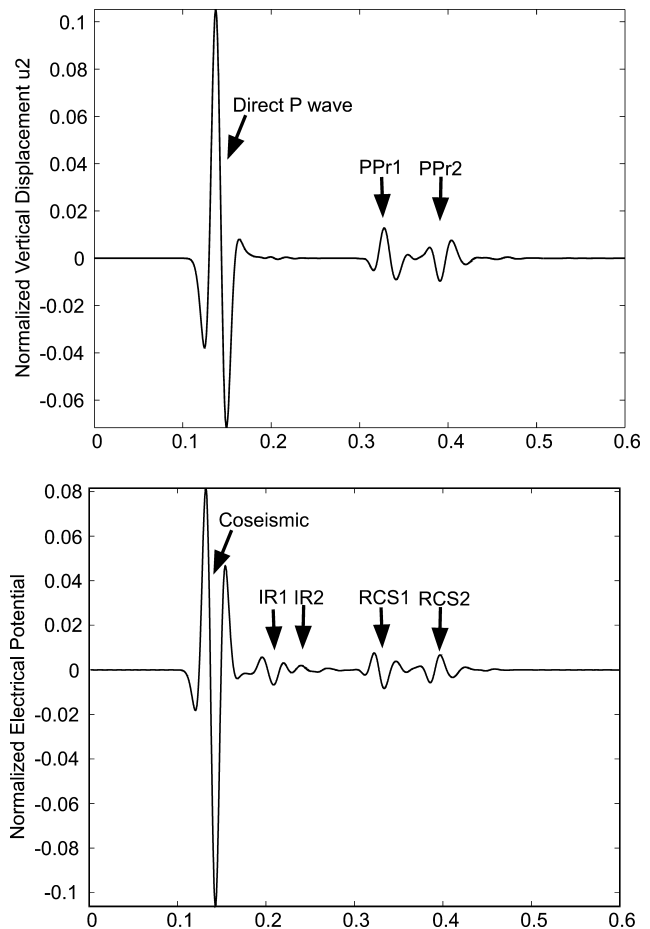


**Figure 6.** Seismogram and electrogram at an electrode (receiver P1 in Fig. 4). The strongest signal on the electrogram corresponds to the coseismic disturbance associated with the direct wave (see Fig. 4). RCS1 and RCS2 stand for the coseismic disturbances associated with the reflected  $P$  waves (see Fig. 1). IR1 and IR2 stand for the two seismoelectric disturbances associated with the seismoelectric conversions at the top and bottom of the reservoir.

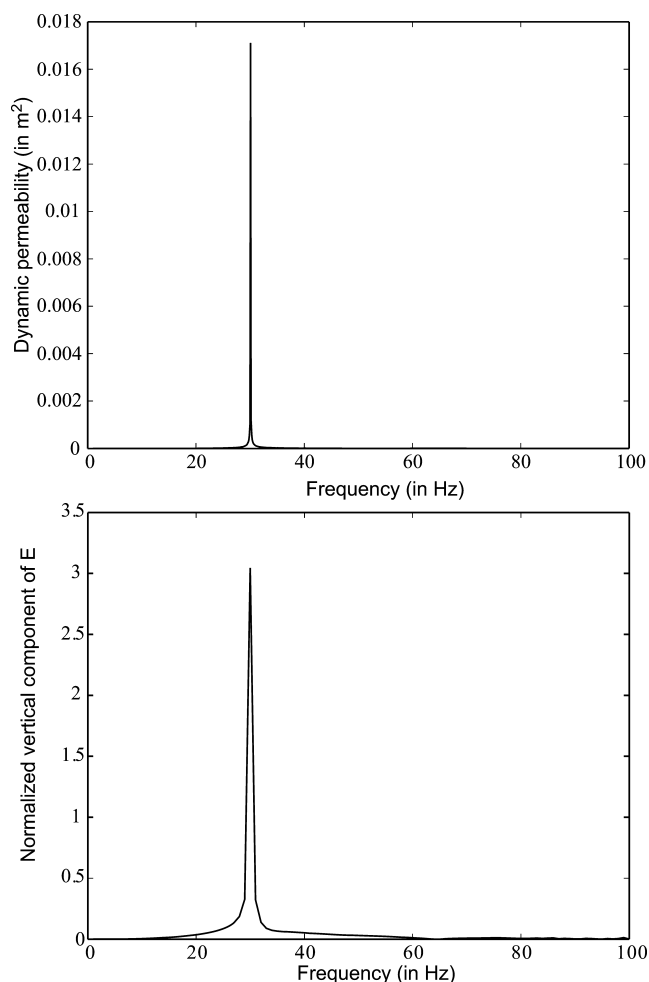


**Figure 7.** Results of the second numerical experiment using the same geometry as in Fig. 4. The fluid of the reservoir is viscoelastic. The source function is a Dirac and we investigate the electrical response in the frequency band (1–100 Hz). The dynamic permeability versus frequency shows the relaxation peak associated with the resonance of the viscoelastic fluid. The peak of the vertical component of the electrical field  $E$  at a remote self-potential station located at  $x = 150$  m and  $y = 0$  m.

(2) Resonance of this solvent occurs in a spectrum of frequencies that depends on its composition. The distribution of the relaxation times of such a fluid can be described by a Cole–Cole distribution. For heavy oils and DNAPL, the resonance frequencies belongs to the seismic band used by conventional seismic methods (10–100 Hz).

(3) If the porous body is excited by seismic waves with frequencies inside this frequency band of resonance of the viscoelastic fluid, the current density associated with the movement of the viscoelastic solvent can be very strong with an enhancement of the streaming potential coupling coefficient of several orders of magnitude with respect to its value at low frequencies. In all the spectrum of frequencies, the source current density, in turn, creates electromagnetic disturbances that can diffuse away from the source of current density. If we are close enough to the source volume of current, the electromagnetic problem can be considered in the quasi-static limit of the Maxwell equations.

(4) A new type of shear wave has been discovered. This new shear wave is controlled by the mechanical properties of the viscoelastic fluid and is related to the resonance of the fluid and its ability to bear

shear stresses. This resonance creates a resonance in the electrical field of electrokinetic nature that may be strongly amplified by several orders of magnitudes.

Future works will be dedicated (1) to the check of the present laboratory in the laboratory and in the field and (2) to the extension of the theory to the case where the pore space of a porous material is filled with two immiscible fluid phases like water and oil looking at the effect of the wettability of the oil phase upon the seismoelectric response.

## ACKNOWLEDGMENTS

We thank Terry Young for his support at CSM. We thank Kasper van Wijk and one anonymous referee for their very constructive reviews and Mark Everett for his work as Associate Editor.

## REFERENCES

- Alkafeef, S., Gochin, R.J. & Smith, A.L., 2001. The effect of double layer overlap on measured streaming currents for toluene flowing through sandstone cores, *Coll. Surfaces A: Physiochem. Eng. Aspects*, **195**, 77–80.
- Alkafeef, S.F. & Smith, A.L., 2005. Asphaltene adsorption isotherm in the pores of reservoir rock cores, in *Paper 93188 Presented at the SPE International Symposium on Oil field Chemistry*, Houston.
- Alkafeef, S.F., Algharaib, M.K. & Alajmi, A.F., 2006. Hydrodynamic thickness of petroleum oil adsorbed layers in the pores of reservoir rocks, *J. Coll. Interf. Sci.*, **298**, 13–19.
- Anderson, W.G., 1986. Wettability literature survey. Part 1: rock/oil/brine interactions and the effects of core handling on wettability, *J. Petrol. Tech.*, **38**, 1125–1144.
- Behura, J., Batzle, M., Hofmann, R. & Dorgan, J., 2007. Heavy oils: their shear story, *Geophysics*, **72**(5), E175–E183.
- Biot, M.A., 1962a. Generalized theory of acoustic propagation in porous dissipative media, *J. acoust. Soc. Am.*, **34**(9), 1254–1264.
- Biot, M.A., 1962b. Mechanics of deformation and acoustic propagation in porous media, *J. appl. Phys.*, **33**(4), 1482–1498.
- Bolève, A., Revil, A., Janod, F., Mattiuzzo, J.L. & Jardani, A., 2007. Forward modeling and validation of a new formulation to compute self-potential signals associated with ground water flow, *Hydrol. Earth Syst. Sci.*, **11**(5), 1661–1671.
- Buckley, J.S. & Liu, Y., 1998. Some mechanisms of crude oil/brine/solid interactions, *J. Petrol. Sci. Eng.*, **20**, 155–160.
- Butler, K.E., Russell, R.D., Kepic, A.W. & Maxwell, M., 1996. Measurement of the seismoelectric response from a shallow boundary, *Geophysics*, **61**, 1769–1778.
- Castrejon-Pita, J.R., Del Río, J.A. & Huelsz, G., 2003. Experimental observations of dramatic differences in the dynamic response of Newtonian and Maxwellian fluids, *Phys. Rev. E*, **68**(4), 046301.
- Cole, K.S. & Cole, R.H., 1941. Dispersion and absorption in dielectrics, *J. Chem. Phys.*, **9**, 341–351.
- Cosenza, P., Ghorbani, A., Florsch, N. & Revil, A., 2007. Effects of drying on the low-frequency electrical properties of Tournemire argillites, *Pure appl. Geophys. (PAGEOPH)*, **164**(10), 2043–2066, doi:10.1007/s00024-007-0253-0.
- Crespy, A., Revil, A., Linde, N., Byrdina, S., Jardani, A., Bolève, A. & Henry, P., 2008. Detection and localization of hydromechanical disturbances in a sandbox using the self-potential method, *J. geophys. Res.*, **113**, B01205, doi:10.1029/2007JB005042.
- Dahlen, F.A. & Tromp, J., 1998. *Theoretical Global Seismology*, Princeton University Press, Princeton.
- Dante, R.C., Geffroy, E. & Chavez, A.E., 2007. Viscoelastic models for Mexican heavy crude oil and comparison with a mixture of heptadecane and eicosane. Part II, *Fuel*, **86**, 2403–2409.
- De Groot, S.R. & Mazur, P., 1984. *Non-Equilibrium Thermodynamics*, Dover, New York, 510 pp.

- Delgado, A.V., González-Caballero, F., Hunter, R.J., Koopal, L.K. & Lyklema, J., 2007. Measurement and interpretation of electrokinetic phenomena, *J. Coll. Interf. Sci.*, **309**, 194–224.
- Dupuis, J.C., Butler, K.E. & Kopic, A.E., 2007. Seismoelectric imaging of the vadose zone of a sand aquifer, *Geophysics*, **72**(6), A81–A85.
- Fourie, F.D., 2003. Application of Electroseismic Techniques to Geohydrological Investigations in Karoo Rocks, *PhD thesis*. University of the Free State, Bloemfontein, South Africa, 195 pp.
- Frenkel, J., 1944. On the theory of seismic and seismoelectric phenomena in a moist soil, *J. Phys. (Soviet)*, **8**(4), 230–241.
- Garambois, S. & Dietrich, M., 2001. Seismoelectric wave conversions in porous media: field measurements and transfer function analysis, *Geophysics*, **66**(5), 1417–1430.
- Garambois, S. & Dietrich, M., 2002. Full waveform numerical simulations of seismoelectromagnetic wave conversions in fluid-saturated stratified porous media, *J. geophys. Res.*, **107**(B7), doi:10.1029/2001JB000316.
- Gassmann, F., 1951. Über die elastizität poröser medien, *Vierteljahrsschr. Naturforsch. Ges. Zuerich*, **96**, 1–23.
- Huang, Q., 2002. One possible generation mechanism of co-seismic electric signals, *Proc. Japan Acad.*, **78**(7B), 173–178.
- Huang, Q. & Liu, T., 2006. Earthquakes and tide response of geoelectric potential field at the Nijijima station, *Chin. J. Geophys.*, **49**(6), 1745–1754.
- Jardani, A. & Revil, A., 2009. Stochastic joint inversion of temperature and self-potential data, *Geophys. J. Int.*, **179**(1), 640–654, doi:10.1111/j.1365-246X.2009.04295.x.
- Jardani, A., Revil, A., Slob, E. & Sollner, W., 2010. Stochastic joint inversion of 2D seismic and seismoelectric signals in linear poroelastic materials, *Geophysics*, in press.
- Johnson, D.L., 1986. Recent developments in the acoustic properties of porous media, in *Proceedings of the international school of physics « Enrico Fermi » course XCIII Frontiers in physical acoustics*, pp. 255–290, ed. Sette, D., Amsterdam, North-Holland.
- Jouniaux, L. & Pozzi, J.P., 1995. Streaming potential and permeability of saturated sandstones under triaxial stress—Consequences for electrotelluric anomalies prior to earthquakes, *J. geophys. Res.*, **100**(B6), 10197–10209.
- Kopic, A.W., Maxwell, M. & Russell, R.D., 1995. Field trials of a seismoelectric method for detecting massive sulfides, *Geophysics*, **60**(02), 365–373.
- Kulesa, B., Murray, T. & Rippin, D., 2006. Active seismoelectric exploration of glaciers, *Geophys. Res. Lett.*, **33**, L07503, doi:10.1029/2006GL025758.
- Leroy & Revil, A., 2009. Spectral induced polarization of clays and clayrocks, *J. geophys. Res.*, **114**, B10202, doi:10.1029/2008JB006114.
- Leroy, P., Revil, A., Altmann, S. & Tournassat, C., 2007. Composition of the interstitial pore water of charged porous media. Theory and application to the Callovo-Oxfordian argillite, *Geochim. cosmochim. Acta.*, **71**(5), 1087–1097, doi:10.1016/j.gca.2006.11.009.
- Leroy, P., Revil, A., Kemna, A., Cosenza, P. & Gorbani, A., 2008. Spectral induced polarization of water-saturated packs of glass beads, *J. Coll. Interface Sci.*, **321**(1), 103–117.
- Linde, N., Jougnot, D., Revil, A., Matthäi, S.K., Arora, T., Renard, D. & Doussan, C., 2007. Streaming current generation in two-phase flow conditions, *Geophys. Res. Lett.*, **34**(3), L03306, doi:10.1029/2006GL028878.
- Lorentz, H.A., 1904. Electromagnetic phenomena in a system moving with any velocity smaller than that of light, in *KNAW Proceedings*, **6**, 1903–1904, Amsterdam, pp. 809–831.
- Martner, S.T. & Sparks, N.R., 1959. The electroseismic effect, *Geophysics*, **24**(02), 297–308.
- Maxwell, J.C., 1885. *Traité d'Électricité et de Magnétisme*, Gauthier-Villars, Tome I.
- Migunov, N. & Kokorev, A., 1977. Dynamic properties of the seismoelectric effect of water saturated rocks, *Izvestiya, Earth Phys.*, **13**(6), 443–446.
- Mikhailov, O.V., Haartsen, M.W. & Toksoz, M.N., 1997. Electroseismic investigation of the shallow subsurface: field measurements and numerical modeling, *Geophysics*, **62**(01), 97–105.
- Mikhailov, O.V., Queen, J. & Toksoz, M.N., 2000. Using borehole electroseismic measurements to detect and characterize fractured (permeable) zones, *Geophysics*, **65**(4), 1098–1112.
- Morency, C. & Tromp, J., 2008. Spectral-element simulations of wave propagation in porous media, *Geophys. J. Int.*, **175**, 301–345.
- Nagao, T. *et al.*, 2002. Electromagnetic anomalies associated with 1995 Kobe earthquake, *J. Geodyn.*, **33**(4-5), 401–411.
- Neev, J. & Yeatts, F.R., 1989. Electrokinetic effects in fluid-saturated poroelastic media, *Phys. Rev. B*, **40**(13), 9135–9141.
- Pengra, D.B., Li, S.X. & Wong, P.-Z., 1999. Determination of rock properties by low-frequency AC electrokinetics, *J. geophys. Res.*, **104**(B12), 29 485–29 508.
- Pride, S., 1994. Governing equations for the coupled electromagnetics and acoustics of porous media, *Phys. Rev. B*, **50**(21), 15 678–15 696.
- Revil, A., 2007. Thermodynamics of transport of ions and water in charged and deformable porous media, *J. Coll. Interf. Sci.*, **307**(1), 254–264.
- Revil, A. & Leroy, P., 2004. Governing equations for ionic transport in porous shales, *J. geophys. Res.*, **109**, B03208, doi:10.1029/2003JB002755.
- Revil, A. & Linde, N., 2006. Chemico-electromechanical coupling in microporous media, *J. Coll. Interf. Sci.*, **302**, 682–694.
- Revil, A., Cathles, L.M., Losh, S. & Nunn, J.A., 1998. Electrical conductivity in shaly sands with geophysical applications, *J. geophys. Res.*, **103**(B10), 23 925–23 936.
- Revil, A., Schwaeger, H., Cathles, L.M. & Manhardt, P., 1999. Streaming potential in porous media. 2. Theory and application to geothermal systems, *J. geophys. Res.*, **104**(B9), 20 033–20 048.
- Revil, A., Naudet, V., Nouzaret, J. & Pessel, M., 2003. Principles of electrography applied to self-potential electrokinetic sources and hydrogeological applications, *Water Resour. Res.*, **39**(5), 1114, doi:10.1029/2001WR000916.
- Revil, A., Leroy, P. & Titov, K., 2005. Characterization of transport properties of argillaceous sediments. Application to the Callovo-Oxfordian Argillite, *J. geophys. Res.*, **110**, B06202, doi:10.1029/2004JB003442.
- Revil, A., Leroy, P., Gorbani, A., Florsch, N. & Niemeijer, A.R., 2006. Compaction of quartz sands by pressure solution using a Cole–Cole distribution of relaxation times, *J. geophys. Res.*, **111**, B09205, doi:10.1029/2005JB004151.
- Revil, A., Linde, N., Cerepi, A., Jougnot, D., Matthäi, S. & Finsterle, S., 2007. Electrokinetic coupling in unsaturated porous media, *J. Coll. Interf. Sci.*, **313**(1), 315–327.
- Russell, R.D., Butler, K.E., Kopic, A.W. & Maxwell, M., 1997. Seismoelectric exploration, *Leading Edge*, **16**, 1611–1615.
- Sheffer, M., 2007. Forward modeling and inversion of streaming potential for the interpretation of hydraulic conditions from self-potential data, *PhD thesis*. The University of British Columbia.
- Yasufuku, S., Ise, T., Inoue, Y. & Ishioka, Y., 1977. Electrokinetic Phenomena in Electrical Insulating Oil/Impregnated Cellulosic Pressboard Systems, in « Electrical Insulation », *IEEE Trans.*, **EI-12**(5), 370–375, Oxford, UK.
- Zeng, Y.Q., He, J.Q. & Liu, Q.H., 2001. The application of the perfectly matched layer in numerical modeling of wave propagation in poroelastic media, *Geophysics*, **66**, 1258–1266.
- Zhu, Z. & Toksoz, M.N., 1998. Seismoelectric measurements in a fractured borehole model (expanded abstract), *Soc. Expl. Geophys.*, 68th Annual Meeting, BH2.7, 314–317.

## APPENDIX A: STRESS–STRAIN RELATIONSHIPS

According to the rheological behaviour of the pore fluid described in Section 2.1, its effective shear modulus is given in the frequency domain by

$$G_f^*(\omega) = \frac{-(i\omega/\omega_m)^c}{1 - (i\omega/\omega_m)^c} G_f. \quad (\text{A1})$$

The fluid does not bear any shear stress at low frequencies ( $\omega \ll \omega_m$ ) and behaves as a solid sustaining a net shear stress at high frequencies ( $\omega \gg \omega_m$ ). We define the two phase averaged deviators by

$$2\bar{\mathbf{d}}_s \equiv \nabla \bar{\mathbf{u}}_s + \nabla \bar{\mathbf{u}}_s^T - \frac{2}{3} (\nabla \cdot \bar{\mathbf{u}}_s) \bar{\mathbf{I}}, \quad (\text{A2})$$

$$2\bar{\mathbf{d}}_f \equiv \nabla \bar{\mathbf{u}}_f + \nabla \bar{\mathbf{u}}_f^T - \frac{2}{3} (\nabla \cdot \bar{\mathbf{u}}_f) \bar{\mathbf{I}}, \quad (\text{A3})$$

respectively. We introduce a relative deviator as,

$$\bar{\mathbf{d}}_w \equiv \phi (\bar{\mathbf{d}}_f - \bar{\mathbf{d}}_s), \quad (\text{A4})$$

$$2\bar{\mathbf{d}}_w = \nabla [\phi (\bar{\mathbf{u}}_f - \bar{\mathbf{u}}_s)] + \nabla [\phi (\bar{\mathbf{u}}_f - \bar{\mathbf{u}}_s)]^T - \frac{2}{3} (\nabla \cdot [\phi (\bar{\mathbf{u}}_f - \bar{\mathbf{u}}_s)]) \bar{\mathbf{I}}, \quad (\text{A5})$$

$$2\bar{\mathbf{d}}_w = \nabla \bar{\mathbf{w}} + \nabla \bar{\mathbf{w}}^T - \frac{2}{3} (\nabla \cdot \bar{\mathbf{w}}) \bar{\mathbf{I}}, \quad (\text{A6})$$

$$2\dot{\bar{\mathbf{d}}}_w = \nabla \dot{\bar{\mathbf{w}}} + \nabla \dot{\bar{\mathbf{w}}}^T - \frac{2}{3} (\nabla \cdot \dot{\bar{\mathbf{w}}}) \bar{\mathbf{I}}. \quad (\text{A7})$$

The total stress tensor and the fluid phase average stress tensors are given by

$$\bar{\mathbf{T}} = -P\mathbf{I} + \bar{\mathbf{T}}^D, \quad (\text{A8})$$

$$\bar{\mathbf{T}}_f = -\bar{p}_f\mathbf{I} + \bar{\pi}, \quad (\text{A9})$$

where  $P$  is the confining pressure,  $\bar{\mathbf{T}}^D$  is the macroscopic deviatoric stress, and  $\bar{\pi}$  is the phase average deviatoric stress of the pore fluid.

In linear poroelasticity, it is customary to consider two distinct thought experiments to obtain the phase averaged tensors in linear isotropic porous materials. The first experiment corresponds to the case of an ideal drained experiment in which a confining pressure  $P = (1 - \phi)\bar{p}_s$  ( $\bar{p}_s$  is the pressure in the solid phase) and deviatoric stress  $\bar{\mathbf{T}}^D$  are applied to a porous sample with no change in the fluid pressure (e.g. considering an empty or drained porous material). In this case, the bulk deformation of the solid frame, the variation of the porosity, and the deviators are

$$\nabla \cdot \bar{\mathbf{u}}_s(P, 0) = -P/K_{fr}, \quad (\text{A10})$$

$$\Delta\phi(P, 0) = -\left(1 - \frac{K_{fr}}{K_s} - \phi\right) \frac{P}{K_{fr}}, \quad (\text{A11})$$

$$2\bar{\mathbf{d}}_s(\bar{\mathbf{T}}^D, 0) = \frac{\bar{\mathbf{T}}^D}{G_{fr}}, \quad (\text{A12})$$

$$2\phi(\bar{\mathbf{d}}_f)^e(\bar{\mathbf{T}}^D, 0) = \left(1 - \frac{G_{fr}}{G_s} - \phi\right) \frac{1}{G_{fr}} \bar{\mathbf{T}}^D, \quad (\text{A13})$$

where  $G_{fr}$  and  $K_{fr}$  are the shear and bulk moduli of the dry porous frame (in other words the shear and bulk moduli of the skeleton of the material).

In the second thought experiment, we apply a fluid pressure  $\bar{p}_f$  everywhere throughout the pore space and, simultaneously, a confining pressure  $P = \bar{p}_f$  to the external surface of the sample. At the same time, we apply the mean deviatoric stress  $\bar{\pi}$  to the pore

space and, simultaneously, a deviatoric stress  $\bar{\mathbf{T}}^D = \bar{\pi}$  to the external surface of the sample. In this case, the bulk deformation of the solid frame, the variation of the porosity, and the variation of the deviators are given by

$$\nabla \cdot \bar{\mathbf{u}}_s(\bar{p}_f, \bar{p}_f) = -\bar{p}_f/K_s, \quad (\text{A14})$$

$$\Delta\phi(\bar{p}_f, \bar{p}_f) = 0, \quad (\text{A15})$$

$$2\bar{\mathbf{d}}_s(\bar{\pi}, \bar{\pi}) = \frac{\bar{\pi}}{G_s}, \quad (\text{A16})$$

$$2\phi(\bar{\mathbf{d}}_f)^e(\bar{\pi}, \bar{\pi}) = 0. \quad (\text{A17})$$

Using the superposition principle, we add together the results of the two thought experiments discussed. For the general case, the bulk deformation of the solid frame, the variation of the porosity, and the deviator are

$$\nabla \cdot \bar{\mathbf{u}}_s(P, \bar{p}_f) = \nabla \cdot \bar{\mathbf{u}}_s(P - \bar{p}_f, 0) + \nabla \cdot \bar{\mathbf{u}}_s(\bar{p}_f, \bar{p}_f), \quad (\text{A18})$$

$$\Delta\phi(P, \bar{p}_f) = \Delta\phi(P - \bar{p}_f, 0) + \Delta\phi(\bar{p}_f, \bar{p}_f), \quad (\text{A19})$$

$$2\bar{\mathbf{d}}_s(\bar{\mathbf{T}}^D, \bar{\pi}) = 2\bar{\mathbf{d}}_s(\bar{\mathbf{T}}^D - \bar{\pi}, 0) + 2\bar{\mathbf{d}}_s(\bar{\pi}, \bar{\pi}), \quad (\text{A20})$$

$$2\phi(\bar{\mathbf{d}}_f)^e(\bar{\mathbf{T}}^D, \bar{\pi}) = 2\bar{\mathbf{d}}_f(\bar{\mathbf{T}}^D, 0) + 2\bar{\mathbf{d}}_f(\bar{\pi}, \bar{\pi}). \quad (\text{A21})$$

This yields,

$$\nabla \cdot \bar{\mathbf{u}}_s(P, \bar{p}_f) = -\frac{(P - \bar{p}_f)}{K_{fr}} - \frac{\bar{p}_f}{K_s}, \quad (\text{A22})$$

$$\Delta\phi(P, \bar{p}_f) = -\left(1 - \frac{K_{fr}}{K_s} - \phi\right) \frac{P - \bar{p}_f}{K_{fr}}, \quad (\text{A23})$$

$$2\bar{\mathbf{d}}_s(\bar{\mathbf{T}}^D, \bar{\pi}) = \frac{1}{G_{fr}} (\bar{\mathbf{T}}^D - \bar{\pi}) + \frac{\bar{\pi}}{G_s}, \quad (\text{A24})$$

$$2\phi(\bar{\mathbf{d}}_f)^e(\bar{\mathbf{T}}^D, \bar{\pi}) = \left(1 - \frac{G_{fr}}{G_s} - \phi\right) \frac{1}{G_{fr}} (\bar{\mathbf{T}}^D - \bar{\pi}), \quad (\text{A25})$$

and therefore

$$\nabla \cdot \bar{\mathbf{u}}_s(P, \bar{p}_f) = -\frac{P}{K_{fr}} + \alpha \frac{\bar{p}_f}{K_{fr}}, \quad (\text{A26})$$

$$\Delta\phi(P, \bar{p}_f) = -(\alpha - \phi) \frac{P - \bar{p}_f}{K_{fr}}, \quad (\text{A27})$$

$$2\bar{\mathbf{d}}_s(\bar{\mathbf{T}}^D, \bar{\pi}) = \frac{1}{G_{fr}} \bar{\mathbf{T}}^D - \alpha_G \frac{\bar{\pi}}{G_{fr}}, \quad (\text{A28})$$

$$2\phi(\bar{\mathbf{d}}_f)^e(\bar{\mathbf{T}}^D, \bar{\pi}) = (\alpha_G - \phi) \frac{1}{G_{fr}} (\bar{\mathbf{T}}^D - \bar{\pi}), \quad (\text{A29})$$

where  $\alpha = 1 - K_{fr}/K_s$  is the classical Biot coefficient ( $\phi \leq \alpha \leq 1$ ) and  $\alpha_G = 1 - G_{fr}/G_s$  is a newly introduced Biot shear coefficient.

The equation for the porosity variation  $\Delta\phi(P, \bar{p}_f)$  can be written as a function of the increment of the fluid content  $\nabla \cdot \bar{\mathbf{w}}(P, \bar{p}_f)$  using the continuity equation for the mass of the pore fluid. This equation is given by

$$\Delta\phi + \frac{\phi}{K_f} \bar{p}_f + \nabla \cdot \bar{\mathbf{w}} + \phi \nabla \cdot \bar{\mathbf{u}}_s = 0, \quad (\text{A30})$$

$$\nabla \cdot \bar{\mathbf{w}} = (\alpha - \phi) \frac{P - \bar{p}_f}{K_{fr}} - \frac{\phi}{K_f} \bar{p}_f + \phi \frac{P}{K_{fr}} - \phi \alpha \frac{\bar{p}_f}{K_{fr}}, \quad (\text{A31})$$

$$\nabla \cdot \bar{\mathbf{w}} = \alpha \frac{P}{K_{fr}} - \frac{\bar{p}_f}{K_{fr}} \left[ \alpha + \phi \left( \frac{K_{fr}}{K_f} - \frac{K_{fr}}{K_s} \right) \right]. \quad (\text{A32})$$

A similar approach can be undertaken for the deviators. Starting with the definition of the differential deviator  $\bar{\mathbf{d}}_w \equiv \phi(\bar{\mathbf{d}}_f - \bar{\mathbf{d}}_s)$  and using

$$\dot{\bar{\mathbf{d}}}_f = \left( \dot{\bar{\mathbf{d}}}_f \right)^v + \left( \dot{\bar{\mathbf{d}}}_f \right)^e, \quad (\text{A33})$$

$$\dot{\bar{\mathbf{d}}}_f = \frac{1}{2\eta_f^*} \bar{\pi} + \left( \dot{\bar{\mathbf{d}}}_f \right)^e, \quad (\text{A34})$$

where the superscript  $v$  and  $e$  stands for the viscous and elastic contributions, respectively, we obtain

$$-\frac{\phi}{2\eta_f^*} \bar{\pi} + \dot{\bar{\mathbf{d}}}_w + \phi \left[ \dot{\bar{\mathbf{d}}}_s - \left( \dot{\bar{\mathbf{d}}}_f \right)^e \right] = 0, \quad (\text{A35})$$

$$-\frac{\phi}{2\eta_f} (1 - i\omega\tau_m) \bar{\pi} - i\omega \left[ \bar{\mathbf{d}}_w + \phi \left( \bar{\mathbf{d}}_s - \left( \bar{\mathbf{d}}_f \right)^e \right) \right] = 0, \quad (\text{A36})$$

$$2\phi \left( \bar{\mathbf{d}}_f \right)^e + \frac{\phi}{G_f^*} \bar{\pi} + 2\bar{\mathbf{d}}_w + 2\phi \bar{\mathbf{d}}_s = 0, \quad (\text{A37})$$

where we have used  $\tau_m = \eta_f/G_f$  and the Debye approximation for the distribution of the time constant. Using eq. (37), we can write the elastic contribution of the mean deviator in the fluid phase  $2\phi \left( \bar{\mathbf{d}}_f \right)^e \left( \bar{\mathbf{T}}^D, \bar{\pi} \right)$  as a function of the differential deviator  $\bar{\mathbf{d}}_w \left( \bar{\mathbf{T}}^D, \bar{\pi} \right)$ :

$$2\bar{\mathbf{d}}_w = -\alpha_G \frac{\bar{\mathbf{T}}^D}{G_{fr}} + \frac{\bar{\pi}}{G_{fr}} \left[ \alpha_G + \phi \left( \frac{G_{fr}}{G_f^*} - \frac{G_{fr}}{G_s} \right) \right]. \quad (\text{A38})$$

This yields for the non-deviatoric and the deviatoric contributions to the deformation

$$\begin{bmatrix} \nabla \cdot \bar{\mathbf{u}}_s \\ \nabla \cdot \bar{\mathbf{w}} \end{bmatrix} = -\frac{1}{K_{fr}} \begin{bmatrix} 1 & -\alpha \\ -\alpha & \phi \left( \frac{K_{fr}}{K_f} - \frac{K_{fr}}{K_s} \right) + \alpha \end{bmatrix} \cdot \begin{bmatrix} P \\ \bar{p}_f \end{bmatrix}, \quad (\text{A39})$$

$$2 \begin{bmatrix} \bar{\mathbf{d}}_s \\ \bar{\mathbf{d}}_w \end{bmatrix} = \frac{1}{G_{fr}} \begin{bmatrix} 1 & -\alpha_G \\ -\alpha_G & \phi \left( \frac{G_{fr}}{G_f^*} - \frac{G_{fr}}{G_s} \right) + \alpha_G \end{bmatrix} \cdot \begin{bmatrix} \bar{\mathbf{T}}^D \\ \bar{\pi} \end{bmatrix}, \quad (\text{A40})$$

respectively. These results generalize the Frenkel–Biot theory to linear poroelastic bodies filled with a linear generalized Maxwell fluid described by a Cole–Cole model. These equations can be also inverted to give

$$-\begin{bmatrix} P \\ \bar{p}_f \end{bmatrix} = \begin{bmatrix} K_U & C \\ C & C/\alpha \end{bmatrix} \cdot \begin{bmatrix} \nabla \cdot \bar{\mathbf{u}}_s \\ \nabla \cdot \bar{\mathbf{w}} \end{bmatrix}, \quad (\text{A41})$$

$$\begin{bmatrix} \bar{\mathbf{T}}^D \\ \bar{\pi} \end{bmatrix} = \begin{bmatrix} G_U & C_G \\ C_G & C_G/\alpha_G \end{bmatrix} \cdot \begin{bmatrix} 2\bar{\mathbf{d}}_s \\ 2\bar{\mathbf{d}}_w \end{bmatrix}, \quad (\text{A42})$$

where the newly introduced material properties are defined as a function of the properties of the constituents by

$$G_U = \frac{(G_s - G_{fr})^2}{G_s [1 + \phi (G_s/G_f^* - 1)] - G_{fr}} + G_{fr}, \quad (\text{A43})$$

$$C_G = \frac{G_s (G_s - G_{fr})}{G_s [1 + \phi (G_s/G_f^* - 1)] - G_{fr}}, \quad (\text{A44})$$

$$M_G = \frac{G_s^2}{G_s [1 + \phi (G_s/G_f^* - 1)] - G_{fr}}, \quad (\text{A45})$$

and  $M_G = C_G/\alpha_G$ . We check that in the limit where  $G_f^* = 0$ , we obtain  $G_U = G_{fr}$ ,  $C_G = 0$  and  $M_G = 0$  and we recover in this limit the classical equations of poroelasticity. The equations can also be used to generalize the Gassmann substitution formula (see Gassmann 1951) for the undrained bulk and shear moduli

$$K_U = \frac{K_f(K_s - K_{fr}) + \phi K_{fr}(K_s - K_f)}{K_f(1 - \phi - K_{fr}/K_s) + \phi K_s}, \quad (\text{A46})$$

$$G_U(\omega) = \frac{G_f^*(\omega)(G_s - G_{fr}) + \phi G_{fr}[G_s - G_f^*(\omega)]}{G_f^*(\omega)(1 - \phi - G_{fr}/G_s) + \phi G_s}, \quad (\text{A47})$$

where  $G_f^*(\omega)$  is given by eq. (A1).

The two other Biot moduli are classically defined by

$$C = \frac{K_f(K_s - K_{fr})}{K_f(1 - \phi - K_{fr}/K_s) + \phi K_s}, \quad (\text{A48})$$

$$M = \frac{C}{\alpha} = \frac{K_f K_s}{K_f(1 - \phi - K_{fr}/K_s) + \phi K_s}. \quad (\text{A49})$$

Note that at low frequencies

$$\lim_{\omega \rightarrow 0} G(\omega) = G_{fr}, \quad (\text{A50})$$

and therefore we recover the case of a Newtonian fluid for (A46) and (A47).

It is also possible to write eq. (A41) as a function of the Skempton coefficient  $B$  and the undrained bulk modulus  $K_U$

$$\begin{bmatrix} P \\ p_f \end{bmatrix} = -K_U \begin{bmatrix} 1 & B \\ B & B/\alpha \end{bmatrix} \begin{bmatrix} \nabla \cdot \bar{\mathbf{u}}_s \\ \nabla \cdot \bar{\mathbf{w}} \end{bmatrix}, \quad (\text{A51})$$

$$K_U = -\frac{P}{\nabla \cdot \bar{\mathbf{u}}_s} \Big|_{\nabla \cdot \bar{\mathbf{w}}=0} = \frac{K}{1 - B\alpha}, \quad (\text{A52})$$

$$B = \frac{p_f}{P} \Big|_{\nabla \cdot \bar{\mathbf{w}}=0}, \quad (\text{A53})$$

$$\alpha = \frac{1}{B} \left( 1 - \frac{K}{K_U} \right), \quad (\text{A54})$$

and  $C = K_U B$  and  $\alpha$  is the bulk Biot coefficient defined above.

## APPENDIX B: THE FIELD EQUATIONS

We start with the Darcy equation, eq. (41), written in the following form and neglecting the electroosmotic term

$$\frac{\eta_f}{k(\omega)} \dot{\bar{\mathbf{w}}} = -\nabla \bar{p}_f - \rho_f \ddot{\bar{\mathbf{u}}}_s + \mathbf{F}_f. \quad (\text{B1})$$

The dynamic permeability is written as

$$\frac{1}{k(\omega)} \equiv \frac{1 - i(\omega/\omega_c)(1 - (i\omega\tau_m)^c)}{k_0(1 - (i\omega\tau_m)^c)}, \quad (\text{B2})$$

from eq. (42). Using the fact that  $\ddot{\bar{\mathbf{w}}} = -i\omega \dot{\bar{\mathbf{w}}}$ , we can easily rewrite eq. (B1) as eq. (67) where the effective fluid density is given by:

$$\bar{\rho}_f = \rho_f F, \quad (\text{B3})$$

where  $F$  is the formation factor defined by eq. (43). This is the same result than for a viscous Newtonian fluid. Indeed for a viscous Newtonian fluid, the frequency dependent permeability is given by

$$k(\omega) = \frac{k_0}{1 - i\omega/\omega_c}. \quad (\text{B4})$$

where  $\omega_c = \eta_f/(k_0\rho_f F)$  where  $F$  is the formation factor. eq. (B4) is a simplified version of eq. (236) of Pride (1994). Inserting eq. (B4) into eq. (B1) results in eq. (67) with  $\tilde{\rho}_f = \rho_f F$ .

The second point studied in this Appendix is to go from eqs (67) and (68) to eq. (71). In the frequency domain, the stress tensor is written as

$$\begin{aligned} \bar{\mathbf{T}} = & \left( K_U - \frac{2}{3} G_U \right) (\nabla \cdot \bar{\mathbf{u}}_s) \mathbf{I} + \left( C - \frac{2}{3} C_G \right) (\nabla \cdot \bar{\mathbf{w}}) \mathbf{I} \\ & + G_U [\nabla \bar{\mathbf{u}}_s + \nabla \bar{\mathbf{u}}_s^T] + C_G [\nabla \bar{\mathbf{w}} + \nabla \bar{\mathbf{w}}^T], \end{aligned} \quad (\text{B5})$$

For a two 2-D problem, the components of the stress tensor are

$$\bar{\mathbf{T}} \equiv \begin{bmatrix} T_{xx} & T_{xz} \\ T_{zx} & T_{zz} \end{bmatrix} \quad (\text{B6})$$

are given by

$$\begin{aligned} T_{xx} = & \left( K_U - \frac{2}{3} G_U \right) \left( \frac{\partial u_x}{\partial x} + \frac{\partial u_z}{\partial z} \right) \\ & + \left( C - \frac{2}{3} C_G \right) \left( \frac{\partial w_x}{\partial x} + \frac{\partial w_z}{\partial z} \right) \\ & + 2G_U \left( \frac{\partial u_x}{\partial x} \right) + 2C_G \left( \frac{\partial w_x}{\partial x} \right), \end{aligned} \quad (\text{B7})$$

$$\begin{aligned} T_{zz} = & \left( K_U - \frac{2}{3} G_U \right) \left( \frac{\partial u_x}{\partial x} + \frac{\partial u_z}{\partial z} \right) \\ & + \left( C - \frac{2}{3} C_G \right) \left( \frac{\partial w_x}{\partial x} + \frac{\partial w_z}{\partial z} \right) \\ & + 2G_U \left( \frac{\partial u_z}{\partial z} \right) + 2C_G \left( \frac{\partial w_z}{\partial z} \right), \end{aligned} \quad (\text{B8})$$

$$T_{xx} = T_{zz} = G_U \left( \frac{\partial u_x}{\partial z} + \frac{\partial u_z}{\partial x} \right) + C_G \left( \frac{\partial w_x}{\partial z} + \frac{\partial w_z}{\partial x} \right). \quad (\text{B9})$$

with these notations, eqs (67) and (68) yield directly eq. (71). In the special case for which the fluid does not bear any shear stress (Newtonian case), we have  $G_U = G_f$  and  $C_G = 0$  and we recover the classical poroelastic equations.

## APPENDIX C: INVERSE FOURIER TRANSFORM OF THE FREQUENCY DEPENDENT MATERIAL PROPERTIES

We look for an expression of  $b(t) = \eta_f^*(t)/k_0$ ,

$$b(t) = \text{FT}^{-1} \left[ \frac{\eta_f^*(\omega)}{k_0} \right], \quad (\text{C1})$$

$$b(t) = \text{FT}^{-1} \left[ b(\omega) \equiv \frac{\eta_f}{k_0} \frac{1}{1 - (i\omega\tau_m)^c} \right], \quad (\text{C2})$$

where  $\text{FT}^{-1}$  stands for the inverse Fourier transform of a given frequency dependent function. Let start by the simpler case where the distribution of the relaxation time obeys to a Dirac distribution (Debye relaxation,  $c = 1$ ). In this case, we have,

$$\text{FT}^{-1} \left( \frac{\eta_f}{k_0} \frac{1}{1 - i\omega\tau_m} \right) = \frac{\eta_f}{k_0} [1 - \exp(-t/\tau_m)], \quad (\text{C3})$$

The more general case  $c \leq 1$  can be found in Revil *et al.* (2006). It yields,

$$b(t) = \frac{\eta_f}{k_0} \left[ 1 - \sum_{n=0}^{\infty} \frac{(-1)^n \left( \frac{t}{\tau_m} \right)^{nc}}{\Gamma(1 + nc)} \right], \quad (\text{C4})$$

where  $\Gamma()$  is the Gamma function defined by,

$$\Gamma(x) \equiv \int_0^{\infty} u^{x-1} e^{-u} du. \quad (\text{C5})$$

We can easily check that in the case where  $c = 1$ , eq. (C4) is equal to (C3) (Revil *et al.* 2006). We can apply the same approach to the properties of the fluid discussed in Section 2.1. For example, we can determine the inverse Fourier transform of the frequency dependent shear modulus of the fluid defined in Appendix A by eq. (A1),

$$G_f^*(\omega) = - \frac{(i\omega/\omega_m)^c}{1 - (i\omega/\omega_m)^c} G_f, \quad (\text{C6})$$

$$G_f^*(t) = \text{FT}^{-1} G_f^*(\omega). \quad (\text{C7})$$

If the Cole–Cole exponent is equal to 1, we have,

$$G_f^*(t) = G_f \exp(-t/\tau_m). \quad (\text{C9})$$

The more general case  $c \leq 1$  can be found easily as,

$$G_f^*(t) = G_f \sum_{n=0}^{\infty} \frac{(-1)^n \left( \frac{t}{\tau_m} \right)^{nc}}{\Gamma(1 + nc)}. \quad (\text{C10})$$